Ohio University

Athens, Ohio

Aeroelastic Reciprocity: An Indicial Response Formulation

Department of

Mechanical Engineering

Aeroelastic Reciprocity: An Indicial Response Formulation

by

Gary M. Graham
Associate Professor of
Mechanical Engineering

Ohio University
Athens, OH 45701

August, 1995

REPORT DOCUMENTATION PAGE

Form Approved
OMB No. 0704-0188

1. AGENCY USE ONLY (Leave blank)	2. REPORT DATE	3. REPORT TYPE AND DATES COVERED
	8/95	Final Technical, 12/92-8/95

4. TITLE AND SUBTITLE
Aerolastic Reciprocity: An Indicial Response Formulation

5. FUNDING NUMBERS
F49620-93-1-0030
2307/CS

6. AUTHOR(S)
Graham, G.M.

7. PERFORMING ORGANIZATION NAME(S) AND ADDRESS(ES)
Ohio University
Mechanical Eng. Dept.
255 Stocker Center
Athens, OH 45701

8. PERFORMING ORGANIZATION REPORT NUMBER

9. SPONSORING/MONITORING AGENCY NAME(S) AND ADDRESS(ES)
AFOSR
Bolling AFB, DC 20332-6448
NA

10. SPONSORING/MONITORING AGENCY REPORT NUMBER
AFOSR
F 49620-93-1-0030

11. SUPPLEMENTARY NOTES

12a. DISTRIBUTION/AVAILABILITY STATEMENT
Approved for Public Release
Distribution is Unlimited

12b. DISTRIBUTION CODE

13. ABSTRACT (Maximum 200 words)

Part I of this report describes an aeroelastic analysis of the an airfoil test rig in a tow tank. The analysis focuses on the aeroelastic response of the rig undergoing a rapid, small amplitude step-like pitching motion. The loading response to this motion is a laboratory simulation of an airfoil indicial response. The aeroelastic model is based on the mode superposition method for structural systems and linear airfoil theory. The Laplace transform method is used to solve the equations of aeroelasticity in closed form. Part II of this report describes an inverse aeroelastic analysis designed to determine the aerodynamic indicial response from the aeroelastic response. The method provides a theoretically sound procedure for determining the indicial response experimentally, even though the indicial response is defined mathematically as the response to a step motion of diminishing amplitude. Part III describes experimental indicial response results using the present inverse aeroelastic method.

14. SUBJECT TERMS
Aeroelasticity, Indicial Response, Nonlinear Aerodynamics

15. NUMBER OF PAGES
55

16. PRICE CODE

17. SECURITY CLASSIFICATION OF REPORT	18. SECURITY CLASSIFICATION OF THIS PAGE	19. SECURITY CLASSIFICATION OF ABSTRACT	20. LIMITATION OF ABSTRACT
U	U	U	

Table of Contents

AEROELASTIC RECIPROCITY: AN INDICIAL RESPONSE FORMULATION

Introduction

The present report describes a continuation of research initiated and reported under grant AFOSR-89-0502. The focus of the research has been an experimental and analytical investigation of airfoil indicial response aerodynamics as related to the convolution integral formulation for unsteady airfoil loading.

The convolution integral formulation for the lift on a flat plate airfoil in arbitrary motion has been derived in Reference[1]. The formulation requires an indicial lift function which by definition is the transient lift response to a step change in angle of attack. The indicial lift response for a flat plate airfoil experiencing a step change in angle of attack due to plunge was first derived by Wagner. In Reference [1], Wagner's function is derived under the assumption of small perturbations using a Fourier integral of Theodorsen's function for harmonic motions. At the onset of the step Wagner's function jumps instantaneously to one-half the steady state lift. Also derived in Reference[1] is Kussner's function for the lift on a flat plate airfoil entering a sharp-edged gust. The initial lift in this case is zero and approaches steady state as the gust overtakes the airfoil. In the case of a 2D airfoil of finite thickness, Reference [2] shows that for an airfoil having a trailing edge with a finite angle of convergence the indicial lift at the step onset is zero. This suggests that the subsequent transient lift for finite airfoils at small incidence may be similar in form to Kussner's function. Reference [2] cites other numerical studies for finite airfoils which appear to agree with the zero initial lift result. Reference [3] uses the Laplace transform method to derive the lift transfer function for a number of airfoil motions. The Laplace domain formulation includes the indicial lift function and results are presented using Kussner's function to describe the indicial lift.

Reference [4] describes a tow tank study designed to measure the normal force response of a NACA 0015 airfoil experiencing sudden step-like changes in angle of attack by rotation about the quarter. The motivation for these experiments was to study airfoil indicial response aerodynamics as defined in the theory of nonlinear mathematical modeling for aerodynamic systems [5]. These experiments involved strain gauge load cell measurements of the transient normal force loading on an airfoil undergoing a sudden change in angle of attack of approximately $\Delta\alpha = \pm 1^{\circ}$. The angle of attack prior to the step onset (α_o) was steady and was varied from run-to-run over the range $2^{\circ} < \alpha_o < 60^{\circ}$.

In the experiments of Reference [4] the test rig may experience large inertial and aerodynamic loading due to the rapid starting and stopping required to impart the step. Therefore, an important issue is the degree to which aeroelastic reactions deform the structure thereby influencing the output of the strain gauge bridge. Knowledge of these reactions is useful in comparing these strain gauge data with the theoretical indicial responses of Wagner and Kussner. Part I of this report describes an aeroelastic analysis of the Ohio University tow tank test rig. The model is based on the mode superposition method for structural systems and classical linear airfoil theory. The Laplace transform method is used to solve the equations of aeroelasticity in closed form.

Part II of this report describes an inverse aeroelastic analysis designed to determine the aerodynamic indicial response from the aeroelastic response. The method provides a theoretically sound procedure for determining

the indicial response experimentally, even though the indicial response is defined mathematically as the response to a step motion of diminishing amplitude. Part III describes indicial responses computed with the method of Part II using tow tank strain gauge data.

Ohio University Tow Tank

A schematic of the O.U. tow tank is shown in Figure 1a. The facility consists of a large tank with a six inch chord NACA 0015 airfoil suspended vertically in the water with a submerged length of 42.0 inches. A carriage moves in translation at 2 ft/s (Re = 9.5E4) along roller bearings fixed to I-beams which span the tank. The airfoil is driven in rotation by a drive shaft fixed to the airfoil quarter chord at one end, and coupled to a 3.5 hp stepper motor/gear box apparatus at the other end. Figure 1b shows details of the drive shaft and airfoil. Shown here are dimensions in inches, and a numbering scheme (1 through 23) defined for the purpose of discretizing the mass of the structure as will be discussed in detail. The drive shaft has a number of variations in cross section over the length of the shaft which must be considered in modeling the aeroelastic response of the structure. Near the middle of the drive shaft is a machined rectangular section which has a strain gauge load cell adhered to the shaft. The load cell section is discretized into mass elements 5 through 9 with the strain gauges located at the centroid of element 7. The strain gauge circuit is electrically compensated to be sensitive to chord normal forces only. The upper most mass element 1 is made of steel while all other parts are aluminum. The modulus of elasticity (E) for steel was taken to be 30×10^6 psi, and for the aluminum was measured to be 7.3×10^6 psi. The modulus of rigidity (G) was taken to be 10×10^6 psi for the steel and for aluminum 4×10^6 psi. The area moment of inertia of the airfoil about the chord line is 0.12 in^4 and the center of mass of the airfoil is located 1.335 inches aft of the pitch axis at the quarter chord. The polar moment of inertia of the airfoil about the pitch axis is 6.71 in^4. The densities of steel and aluminum were taken to be 0.3 and 0.1 lb_m/in^3. The mass of the airfoil per unit length is 0.1598 lb_m/in.

Theoretical Linear Normal Force Response for Small Angles of Attack

In an incompressible flow at small incidence, the theoretical linear normal force coefficient response of an airfoil given an instantaneous step change in angle of attack by *rotation* about the quarter chord is related to the indicial lift function , $\Gamma(t)$, and is given by:

$$C_N(t) = C_{No} + \pi\Delta\alpha \left[\delta(t-0) + \frac{1}{2}\delta'(t-0) \right] + 2\pi\Delta\alpha \left(\Gamma(t) - \Gamma'(t) \right) \qquad (1a)$$

where C_{No} is the initial normal force, $\Delta\alpha$ is the step amplitude, δ' is the time derivative of the Dirac delta function δ, and Γ' is the time derivative of Γ. The first two terms in brackets in Equation (1) are generalized functions [6] which describe the noncirculatory component of the loading, while the last group of terms gives the circulatory component. For a flat plate airfoil the indicial function can be represented by a two pole curve fit to Wagner's function:

$$\Gamma(t) = \left[1 - 0.165e^{-.0455t} - 0.335e^{-.3t} \right] \qquad (1b)$$

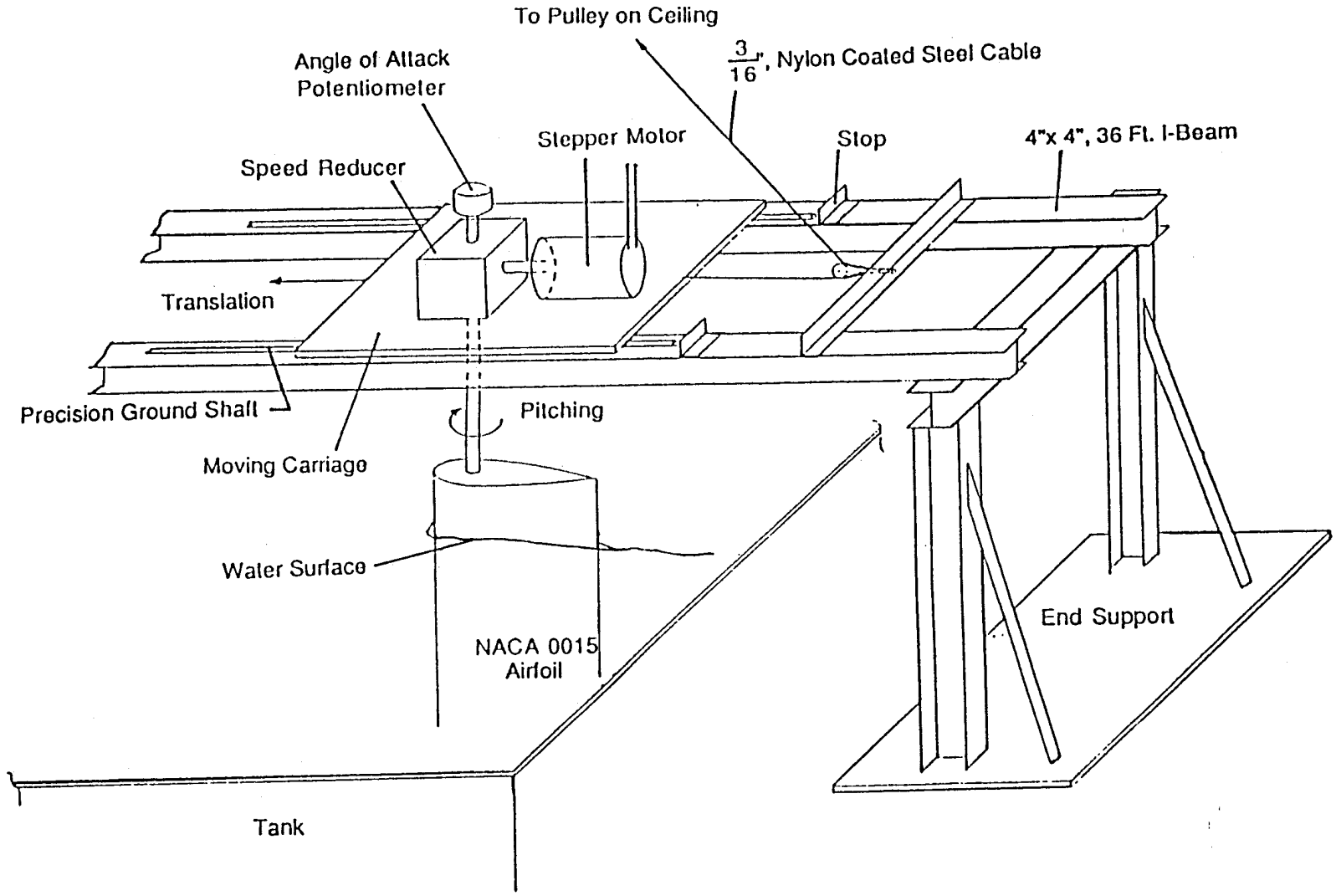

Figure 1a. Ohio University Tow Tank Facility

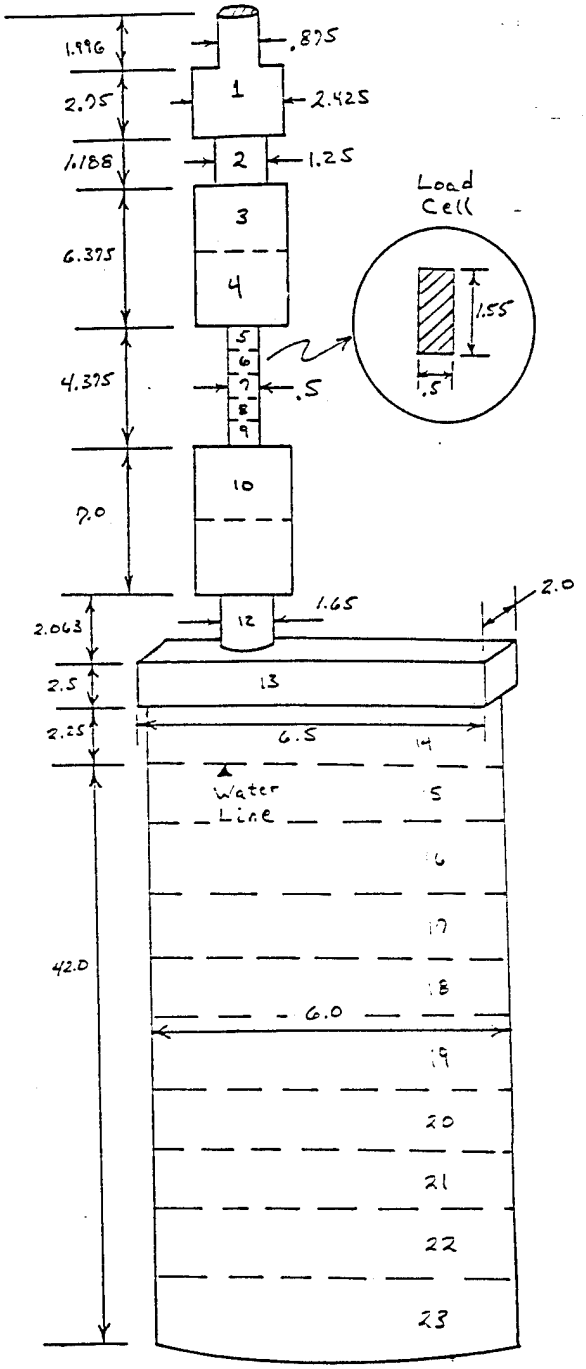

Figure 1b. Test rig

Other workers have used Kussner's function for the lift on an airfoil penetrating a sharp-edged gust, in which case:

$$\Gamma(t) = [\, 1 - 0.5e^{-.13t} - 0.5e^{-t} \,] \qquad (1c)$$

Transient normal force responses of a NACA 0015 airfoil undergoing sudden step-like changes in angle of attack by rotation have been measured in the Ohio U. tow tank. Figure 2 shows angle of attack data for a typical run (small spikes are electrical noise). The onset angle is 2.09° and the step amplitude is approximately +1.25°. The motion resembles, to a reasonable approximation, a small amplitude ramp motion. Equation (1) is compared below with the experimental strain gauge data corresponding to the motion of Figure 2. To facilitate the comparison, the coefficient 2π (for a flat plate airfoil) on the circulatory part in Equation (1) has been replaced by the static normal force curve slope (for the present NACA 0015) which has been measured in an independent test [4]. This substitution is necessary for the response of Equation (1) to approach the same steady state as the experimental response.

Part I: Aeroelastic Analysis

The present analysis is based on the mode superposition method for a forced structural dynamic response [7], and linear airfoil theory formulated in terms of the convolution integral for the loading on an airfoil in arbitrary motion [1]. The structure to be modeled has been shown in Figure 1b. Because the pitch axis (drive shaft axis) does not coincide with the center of mass of the lower part of the structure (mass elements 13-23), it is necessary to consider the coupling between the chord normal and torsional aeroelastic degrees of freedom.

System Representation

As illustrated in Figure 1b, the structure has been discretized into 23 mass elements which are considered to be concentrated at the centroid of each element. Under the influence of aeroelastic loading, the masses will deflect normal to the airfoil chord referred to here as the normal degree of freedom (NDOF), as well as in torsion about the pitch axis hereafter referred to as the TDOF. The lowest nine masses (15-23) represent the submerged portion of the airfoil, and masses 5 through 9 correspond to the rectangular cross section load cell. Masses are concentrated on the load cell to obtain good resolution of the deformation and strain. In the TDOF, the mass elements are replaced by polar mass moment of inertia elements. For the TDOF analysis, the structure is discretized in the same way as the NDOF for elements 1 through 12, however, elements 13 through 23 are lumped into a single inertia element giving a total of 13 inertia elements. The reduction in elements in the TDOF is based on the fact that the torsional stiffness of both the mounting block (element 13) and airfoil are much larger than the drive shaft, and consequently the mounting block and entire airfoil experience nearly the same TDOF deflection. The resulting discretized structure may be described mathematically in terms of a diagonal mass matrix [M], a symmetric NDOF flexibility matrix [AN], a diagonal polar mass moment of inertia matrix [J], and a symmetric TDOF flexibility matrix [AT]. The flexibility coefficient AN(i,j) is by definition the deflection of mass i due to a unit force applied at mass j, while AT(i,j) gives the angular rotation of polar inertia i due to a unit torque applied to inertia j. The matrix [AN] has been computed by assuming the structure to deform as a cantilever beam and integrating the second order differential equation for the elastic beam curvature

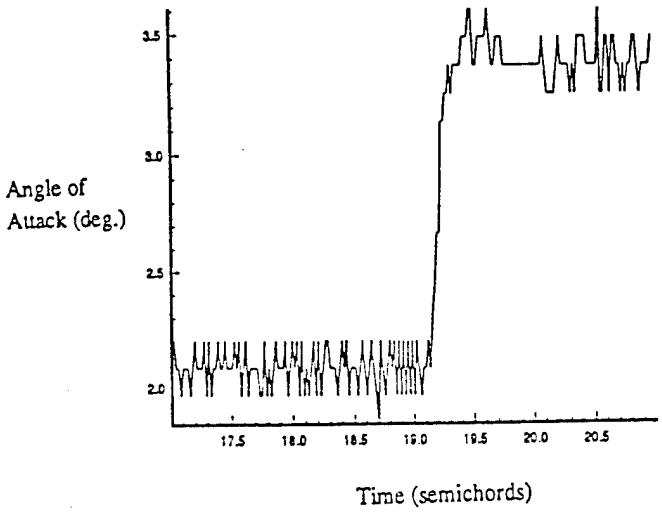

Figure 2. Angle of Attack Data for Indicial Response Test

[8]. A condition of continuous slope is applied at discontinuities in area moment of inertia of the drive shaft. The matrix [AT] has been computed using mechanics for shafts in torsion[9]. The analytically derived flexibility matrices have been validated to some extent by loading the structure and measuring the deflection at selected points. The NDOF stiffness matrix [KN] and TDOF stiffness matrix [KT] are computed by inverting [AN] and [AT], respectively, and has been done using an IMSL subroutine.

Eigenvalue Problem

The system matrices above have been used to solve the eigenvalue problem for the natural frequencies and mode shape vectors of the system. The eigenvalues (natural frequencies) and eigenvectors (modal vectors) have been computed using the IMSL subroutine EVCRG. In the mode superposition analysis, the two lowest NDOF modes (NDOF1 and NDOF2) have been used, while for the TDOF only the lowest fundamental mode has been retained. The corresponding modal vectors are plotted in Figure 3 and given numerically in Table 1. The modal vectors are designated below as ϕ_{N1}, ϕ_{N2}, and ϕ_T for the NDOF1, NDOF2, and TDOF, respectively.

Table 1. Modal Vectors for NDOF1, NDOF2, and TDOF

i	ϕ_{N1}	ϕ_{N2}	ϕ_T
1	0.003	-0.002	0.0392
2	0.0011	-0.0073	0.0647
3	0.0025	-0.0156	0.0983
4	0.0156	-0.0922	0.1178
5	0.0229	-0.1332	0.2080
6	0.0270	-0.1542	0.3687
7	0.0318	-0.1778	0.5294
8	0.0375	-0.2038	0.6900
9	0.0439	-0.2319	0.8507
10	0.0620	-0.3067	0.9417
11	0.0928	-0.4287	0.9629
12	0.1189	-0.5252	0.9867
13	0.1416	-0.6019	1.0000
14	0.1661	-0.6790	1.0
15	0.2090	-0.7609	1.0
16	0.2803	-0.7984	1.0
17	0.3642	-0.7455	1.0
18	0.4581	-0.6027	1.0
19	0.5595	-0.3783	1.0
20	0.6661	-0.0871	1.0
21	0.7760	0.2522	1.0

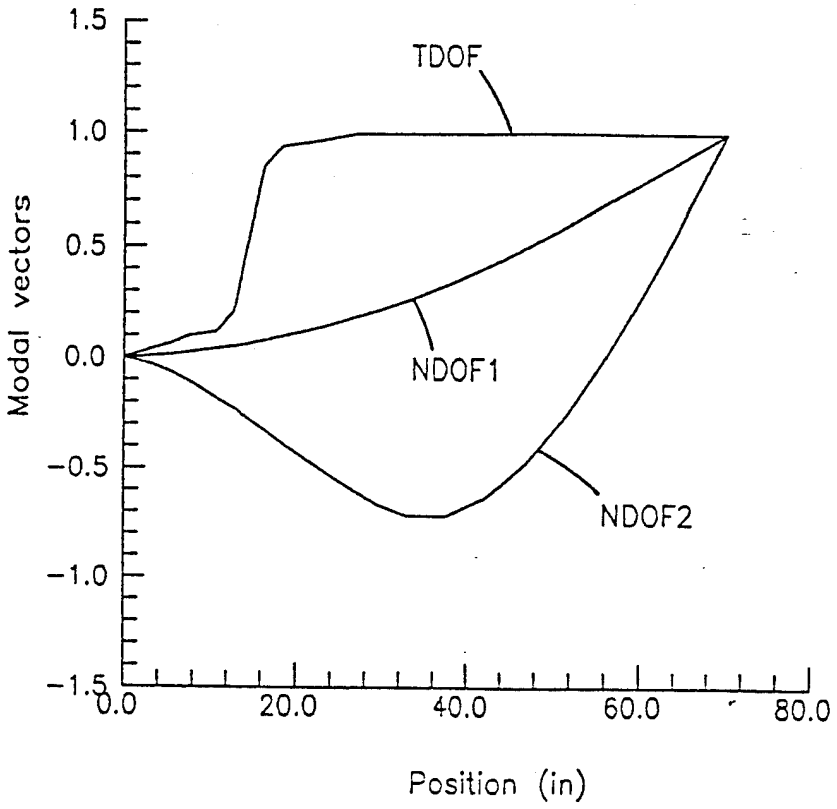

Figure 3. Modal Vectors.

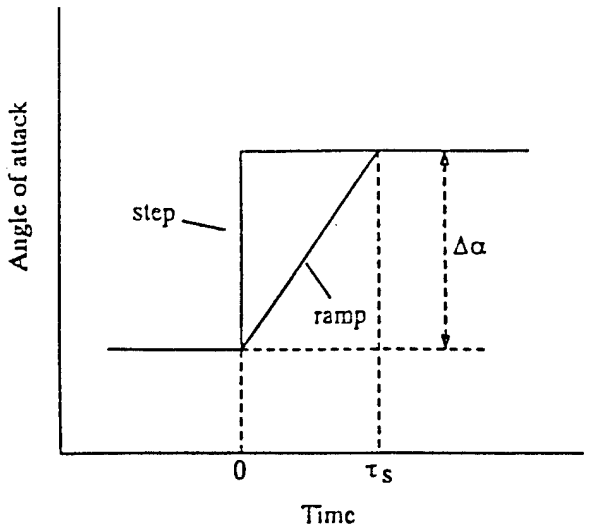

Figure 4. Step and Ramp Input Motions

22	0.8877	0.6202	1.0
23	1.0000	1.0000	1.0

*The position of element i is located at the centroid of the element (see Figure 1b).

The nondimensional natural frequencies ($\omega b/U$, b=semichord, U=velocity) for the NDOF modes were computed to be $\omega_{N1} = 6.374$ and $\omega_{N2} = 26.985$, and for the TDOF $\omega_T = 65.782$. Notice that the initial part of the angle of attack data (the ramp) of Figure 2 has a slope nearly the same as a sine function with a nondimensional frequency near 50. This frequency is, in a sense, the excitation frequency. Because the NDOF2 and TDOF natural frequencies are near the excitation frequency, it is appropriate to consider these modal responses. As seen below, apparent mass and inertia effects tend to reduce the *aeroelastic* frequencies even further.

Structural Dynamics Model

The aeroelastic structural response of the O.U. test rig has been modeled using the mode superposition method and classical linear airfoil theory. For modeling the rigid body rotation of the rig, a rotation degree of freedom (RDOF) is introduced. The RDOF is used to simulate the change in angle of attack of the structure due to the rotation imparted by the stepper motor. The NDOF and TDOF as defined above simulate only deformations relative to the instantaneous position of the top of the drive shaft where both the NDOF and TDOF deflections are always zero.

In the NDOF and TDOF, the deflections of the structure are given by the normalized mode shape vectors multiplied by time dependent modal amplitudes. The total deflection of the structure is defined by:

$$\mathbf{v}_N(t) = \phi_{N1} q_1(t) + \phi_{N2} q_2(t) \qquad (2)$$
$$\mathbf{v}_T = \phi_T g(t)$$
$$\alpha(t) = p(t)$$

where $\mathbf{v}_N$ and $\mathbf{v}_T$ are the deflection vectors in the NDOF and TDOF, respectively, and $\alpha(t)$ describes the RDOF motion. The quantities $q_1(t)$, $q_2(t)$, and $g(t)$ are the modal amplitudes which are the generalized coordinates of the system. The scalar RDOF motion variable p(t) is the magnitude of the nominal angle of attack as the structure is pitched and is an input to the model. This is the angle measured by the rotational potentiometer illustrated in Figures 1a and 2.

Substituting Equations (2) into the equations of motion for the system and using the orthogonality of the modal vectors w.r.t. the system mass and stiffness matrices to uncouple the modal equations [7] yields the following three generalized equations of motion:

$$M_1\ddot{q}_1 + K_1 q_1 = \phi_{N1}^T \mathbf{F} \qquad (3a)$$
$$M_2\ddot{q}_2 + K_2 q_2 = \phi_{N2}^T \mathbf{F} \qquad (3b)$$
$$J\ddot{g} + C_T\dot{g} + K_T g = \phi_T^T \mathbf{T} \qquad (3c)$$

where the generalized system properties are scalar quantities given by:

$$M_1 = \phi_{N1}^T[M]\phi_{N1}\ ,\ M_2 = \phi_{N2}^T[M]\phi_{N2}\ ,\ J = \phi_T^T[J]\phi_T$$
$$K_1 = \phi_{N1}^T[KN]\phi_{N1}\ ,\ K_2 = \phi_{N2}^T[KN]\phi_{N2}\ ,\ K_T = \phi_T^T[KT]\phi_T \qquad (4)$$
$$C_T = 2\zeta_T J\omega_T$$

The damping term in the last of Equations (3) is included to account for a small amount of rotational "play" in the airfoil drive shaft which tends to cause oscillations in TDOF to damp out. In Equation (4), ζ_T is the damping ratio which was estimated to be 0.05 and ω_T is the natural frequency in the TDOF. The solution of Equations (3) for the generalized coordinates $q_1(t)$, $q_2(t)$, and g(t) subject to a prescribed RDOF input parameter p(t), is described below. All terms in Equations 3 have been nondimensionalized based on freestream velocity, semichord length, and the density of water.

Aeroelastic Normal Forces

The normal force acting on the structure is decomposed into a rigid body force vector, $\mathbf{F}_R$, associated with the RDOF, an aeroelastic force vector, $\mathbf{F}_A$, due to time dependent aeroelastic deflections along the span of the airfoil, and an inertial force vector, $\mathbf{F}_I$, so that in Equations (3), $\mathbf{F} = \mathbf{F}_R + \mathbf{F}_A + \mathbf{F}_I$.

The rigid body force vector is the ideal aerodynamic loading response to a step change in angle of attack due to rotation about the quarter chord. These aerodynamic forces are exerted only on the submerged part of the airfoil represented by masses 15 through 23 of Figure 1b. For a given motion input p(t), the vector $\mathbf{F}_R$ at any time, t, at or after the step is given by :

$$F_{Ri} = 0 \qquad , i = 1, 2...14$$
$$F_{Ri}(t) = \pi L_i \{\dot{p}(t) + \frac{1}{2}\ddot{p}(t)\} + C_{N\alpha} L_i \int_0^t (\dot{p}(\tau) + \ddot{p}(\tau))\,\Gamma(t-\tau)\,d\tau \qquad (5)$$
$$, i = 15, 16,...23$$

where $C_{N\alpha}$ is the static normal force curve slope at the step onset angle, L_i is the span of the i^{th} airfoil element (see Fig. 1b), and $\Gamma(t-\tau)$ is the indicial lift response given by either Equation (1b) or Equation (1c). Notice that $\mathbf{F}_R$ is not a function of the generalized coordinates $q_1(t)$, $q_2(t)$, and g(t) since in the ideal response the loading is given by (rigid body) 2-D airfoil theory alone. Notice also that if p(t) is a unit step function of amplitude $\Delta\alpha$ and L_i is unity, Equation (5) becomes identical to Equation (1a) (minus the initial lift C_{No}).

The aeroelastic force vector is also based on the convolution integral formulation for an airfoil in arbitrary motion, and again acts only on the submerged part of the airfoil. For the pitch axis at the quarter chord the loading is:

$$F_{Ai} = 0 \qquad , i = 1, 2,...14$$

$$F_{Ai}(t) = \pi L_i \{-(\phi_{N1i}\,\ddot{q}_1(t) + \phi_{N2i}\,\ddot{q}_2(t)) + \phi_{Ti}\,(\dot{g}(t) + \tfrac{1}{2}\ddot{g}(t))\} +$$

$$C_{N\alpha} L_i \int_0^t [-(\phi_{N1i}\,\ddot{q}_1(\tau) + \phi_{N2i}\,\ddot{q}_2(\tau)) + \phi_{Ti}\,(\dot{g}(\tau) + \ddot{g}(\tau))]\,\Gamma(t-\tau)\,d\tau \qquad (6)$$

$$, i = 15,16,...23$$

where ϕ_{N1i} and ϕ_{N2i} are the values of the NDOF1 and NDOF2 mode shapes at element i, respectively, and ϕ_{Ti} is the value of the TDOF mode shape. The negative sign on the NDOF terms is due to the sign convention adopted. The non-integral terms are the so called apparent mass terms since they may be moved to the LHS and combined with the mass term.

The inertial loading arises from the fact that the centroids of masses 13 through 23 do not coincide with the pitch axis. Thus, angular acceleration about the pitch axis produces an inertial normal force which acts at the centroid. The inertial force vector is:

$$F_{Ii} = 0 \qquad , i = 1, 2,...12$$

$$F_{Ii}(t) = m_i r_i \{\phi_{Ti}\,\ddot{g}(t) + \ddot{p}(t)\} \qquad , i = 13,14,...23 \qquad (7)$$

where m_i is the mass of element i and r_i is the distance from the pitch axis to the centroid.

Aeroelastic Moments

The moments acting on the inertial elements of Figure 1b are also decomposed into a rigid body moment vector, $\mathbf{T}_R$, an aeroelastic moment vector, $\mathbf{T}_A$, and an inertial moment vector, $\mathbf{T}_I$, giving a total moment of: $\mathbf{T} = \mathbf{T}_R + \mathbf{T}_A + \mathbf{T}_I$. The rigid body moment and the aeroelastic moment act only on the submerged part of the airfoil. The expressions for these components are simplified by the fact that the circulatory normal force acts at the quarter chord (for a flat plate airfoil) giving a zero moment arm in the present study. For a NACA 0015 airfoil the circulatory normal force (at $Re \sim 10^5$) acts within 2% fraction of chord from the quarter chord and on this basis has been neglected. The rigid body moment for rotation about the quarter chord is:

$$T_{Ri} = 0 \qquad , i = 1, 2,...14$$

$$T_{Ri}(t) = -\pi L_i \{\dot{p}(t) + \tfrac{3}{8}\ddot{p}(t)\} \qquad , i = 15,16,...23 \qquad (8)$$

The aeroelastic moment vector acting on an airfoil in arbitrary motion with the pitch axis at the quarter chord is given by:

$$T_{Ai} = 0 \qquad , i = 1, 2,...14$$

$$T_{Ai}(t) = \pi L_i \{\tfrac{1}{2}(\phi_{N1i}\,\ddot{q}_1(t) + \phi_{N2i}\,\ddot{q}_2(t)) - \phi_{Ti}\,(\dot{g}(t) + \tfrac{3}{8}\ddot{g}(t))\} \qquad (9)$$

$$, i = 15,16,...23$$

The inertial moment vector is:

$$T_{Ii} = J_i \ddot{p}(t) \qquad , i = 1,2,...12$$

$$T_{Ii}(t) = m_i r_i (\phi_{N1i} \ddot{q}_1(t) + \phi_{N2i} \ddot{q}_2(t)) - J_i \ddot{p}(t) \quad (10)$$

$$, i = 13,14,....23$$

where J_i is the mass moment of inertia of element i.

Notice that Equations (3a,b,c) are coupled through the force and moment terms given by Equations (5) through (10).

Input Rigid Body Motion

Two input motions have been considered and are illustrated in Figure 4. The first motion is a step function input of magnitude $\Delta\alpha$ and the second input is small amplitude ramp modeled after the experimental angle of attack of Figure 2. These motions are expressed mathematically by:

$$p(t) = \Delta\alpha\, \mu(t-0) \quad \text{(step)} \quad (11a)$$

$$p(t) = \frac{\Delta\alpha}{\tau_s} t\, (\mu(t-0) - \mu(t-\tau_s)) + \Delta\alpha\, \mu(t-\tau_s) \quad \text{(ramp)} \quad (11b)$$

where μ is the unit step function, and τ_s (=0.13 semichords) is the ramp duration which is determined from the experimental angle of attack data. As will be seen, it will be necessary to take the Laplace transforms of Equations (11a) and (11b) which yields, respectively:

$$P(s) = \frac{\Delta\alpha}{s} \quad \text{(step)} \quad (11c)$$

$$P(s) = \frac{\Delta\alpha}{s^2\tau_s}(1 - e^{-s\tau_s}) \quad \text{(ramp)} \quad (11d)$$

where , s, is the Laplace variable.

Solution of the Generalized Equations of Motion

The Laplace transform method is used to transform the three generalized differential Equations (3a,b,c) into three algebraic equations which are linear in terms of the transformed generalized coordinates. These equations are solved simultaneously for the transformed generalized coordinates as functions of the Laplace variable, s. The inverse Laplace transform is performed to transform these solutions to the time domain to obtain $q_1(t)$, $q_2(t)$, and g(t). The Laplace transform of each of Equations (3) can be done by hand using standard tables. To perform the extensive algebra required in the solution, the computer program MACSYMA has been used. MACSYMA is capable of symbolic mathematics required in the solution of the simultaneous equations in terms of the Laplace variable, s. The resulting equations of motion in the Laplace transform domain are quite long and are omitted here. Once the Laplace transforms of Equations (3) have been done, the solution proceeds by first rearranging, using MACSYMA, the system of three equations into the following form:

$$\begin{bmatrix} A_{11}(s) & A_{12}(s) & A_{13}(s) \\ A_{21}(s) & A_{22}(s) & A_{23}(s) \\ A_{31}(s) & A_{32}(s) & A_{33}(s) \end{bmatrix} \begin{Bmatrix} Q_1(s) \\ Q_2(s) \\ G(s) \end{Bmatrix} = \begin{Bmatrix} F_1(s) \\ F_2(s) \\ F_3(s) \end{Bmatrix} P(s) \tag{12}$$

where $Q_1(s)$ is the Laplace transform of $q_1(t)$, $Q_2(s)$ of $q_2(t)$, and $G(s)$ of $g(t)$. In Equation (12), $P(s)$ is the Laplace transform of the motion input parameter $p(t)$ (Equation (11c) or (11d)). Equation (12) can be solved using Cramer's rule to yield:

$$\{X(s)\} = \{R(s)\} P(s) \tag{13a}$$

where $\{X(s)\}$ is a 3x1 vector given by:

$$\{X(s)\} = \begin{Bmatrix} Q_1(s) \\ Q_2(s) \\ G(s) \end{Bmatrix} \tag{13b}$$

and the 3x1 vector $\{R(s)\}$ is an aeroelastic transfer function which is a function of the Laplace variable , s, only and is given by:

$$R_1(s) = \frac{\begin{vmatrix} F_1(s) & A_{12}(s) & A_{13}(s) \\ F_2(s) & A_{22}(s) & A_{23}(s) \\ F_3(s) & A_{32}(s) & A_{33}(s) \end{vmatrix}}{\begin{vmatrix} A_{11}(s) & A_{12}(s) & A_{13}(s) \\ A_{21}(s) & A_{22}(s) & A_{23}(s) \\ A_{31}(s) & A_{32}(s) & A_{33}(s) \end{vmatrix}}, \quad R_2(s) = \frac{\begin{vmatrix} A_{11}(s) & F_1(s) & A_{13}(s) \\ A_{21}(s) & F_2(s) & A_{23}(s) \\ A_{31}(s) & F_3(s) & A_{33}(s) \end{vmatrix}}{\begin{vmatrix} A_{11}(s) & A_{12}(s) & A_{13}(s) \\ A_{21}(s) & A_{22}(s) & A_{23}(s) \\ A_{31}(s) & A_{32}(s) & A_{33}(s) \end{vmatrix}}, \quad R_3(s) = \frac{\begin{vmatrix} A_{11}(s) & A_{12}(s) & F_1(s) \\ A_{21}(s) & A_{22}(s) & F_2(s) \\ A_{31}(s) & A_{32}(s) & F_3(s) \end{vmatrix}}{\begin{vmatrix} A_{11}(s) & A_{12}(s) & A_{13}(s) \\ A_{21}(s) & A_{22}(s) & A_{23}(s) \\ A_{31}(s) & A_{32}(s) & A_{33}(s) \end{vmatrix}}$$

where the brackets indicate the determinant. It has been found efficacious to perform the necessary algebra so that $R_1(s)$, $R_2(s)$, and $R_3(s)$ are the form of the quotients of two polynomials. This amounts to manipulating Equation (12) so that all of the terms in the square matrix [A] and the terms in the vector {F} are at most polynomials (i.e. not themselves quotients). Quotients will appear in [A] and {F} due to the exponential form of the indicial function $\Gamma(t-t)$. Recalling form Equations (1b) and (1c), the indicial function is of the form: $\Gamma(t) = 1 - Ae^{at} - Be^{bt}$, which has the Laplace transform:

$$\gamma(s) = \frac{1}{s} - \frac{A}{s-a} - \frac{B}{s-b} = \frac{(1-A-B)s^2 + (Ab+Ba-a-b)s + ab}{s(s-a)(s-b)} \tag{13c}$$

The quotient may be eliminated by simply multiplying the entire system of Equations (12) by the denominator of $\gamma(s)$. This will render the terms of [A] and {F} as non-quotients and simplify the Laplace inversion by partial fraction decomposition which follows.

Substitution of a particular input motion, P(s), into Equation (13a) gives the solution for the generalized coordinates in the Laplace domain. For the step input of Equation (11c), the result for each generalized

coordinate is in the form of a quotient of two polynomials in s, wherein the numerator is a tenth order polynomial and the denominator is an eleventh order polynomial. For the ramp motion of Equation (11d) the result is a tenth order divided by a twelfth order polynomial.

In either case, the inverse Laplace transform is accomplished by decomposing the quotients using partial fractions into functions which can be inverted by hand. In the partial fraction decomposition MACSYMA has been used to find the roots of the polynomial in the denominator. In the step input case the denominator has five real roots while in the ramp input the denominator has six real roots with a repeated root at s=0. The real roots arise from the leading constant and the exponential terms in the indicial response function, Γ, and the real roots of the motion function P(s). In both the step and ramp input cases, the denominator further has three pairs of complex conjugate roots which represent the oscillatory (harmonic) response of the structure at the three frequencies associated with the NDOF1, NDOF2, and TDOF. The numerical values of the frequencies of the harmonic response can be traced to the mass (including apparent mass) and stiffness terms in the governing aeroelastic equations. The set of simultaneous equations for the undetermined constants in the partial fraction expansion terms have been solved using direct factorization with maximal column pivoting [10]. Pivoting is recommended since the coefficients in the simultaneous equations vary over several orders of magnitude.

It is worth noting that in the ramp motion input case it is not necessary to use the full form of P(s) as given by Equation (11d). This is because the last exponential term on the right hand side results in an inverse transform identical to the inverse transform of the term which precedes it, but shifted in time by an amount, τ_s. Thus it is only necessary to use $P(s) = \Delta\alpha/s^2\tau_s$ when calculating this case, and subsequently subtracting from this solution an identical solution shifted in time by τ_s. This effect can be seen in the solution presented below as Equation (14b).

For the step input case, the solutions for the generalized coordinates $q_1(t)$, $q_2(t)$, and g(t) can be represented generally by the function f(t) which has the following form:

$$f(t) = A + Be^{bt} + Ce^{ct} + De^{dt} + Fe^{ft} + e^{ht}(G\cos\omega_1 t + H\sin\omega_1 t) + e^{jt}(J\cos\omega_2 t + K\sin\omega_2 t) + e^{mt}(M\cos\omega_3 t + N\sin\omega_3 t) \quad (14a)$$

where the constants are given in the following table. The constants in Tables 2 and 3 were computed using the Wagner function for the indicial lift function, Γ.

Table 2. Constants for Generalized Coordinates for Step Input using Wagner Function

	$q_1(t)$	$q_2(t)$	g(t)
A	1.241e-2	1.196e-4	0
B	-1.417e-3	-3.178e-6	-9.786e-9
C	-6.001e-4	-1.537e-5	7.451e-9
D	-3.162e-3	1.601e-5	-1.531e-7
F	-3.619e-5	-4.268e-5	-2.328e-10
G	8.407e-3	-3.149e-5	-5.536-5
H	2.042e-2	-9.484e-5	-4.836e-5

J	7.314e-4	7.155e-3	-3.273e-4
K	1.476e-4	1.725e-3	-5.791e-5
M	-1.584e-2	-6.993e-3	-2.075e-2
N	-3.740e-4	-1.377e-4	6.344e-4

The remaining constants apply to each of $q_1(t)$, $q_2(t)$, and $g(t)$

$b = -0.04522$

$c = -0.04565$

$d = -0.2877$

$f = -0.29989$

$h = -0.55591$

$j = -0.49752$

$m = -2.71184$

$\omega_1(\text{NDOF1}) = 2.3361$

$\omega_2(\text{NDOF2}) = 12.186$

$\omega_3(\text{TDOF}) = 52.2147$

For the ramp motion input, the solutions for $q_1(t)$, $q_2(t)$, and $g(t)$ in the time domain can be represented by a function of the form: $f(t) - \mu(t-\tau_s) f(t-\tau_s)$ (e.g. $q_1(t) = f(t) - \mu(t-\tau_s) f(t-\tau_s)$), where τ_s is the ramp duration (0.13 semichords), and $\mu(t-\tau_s)$ is the unit step function. As has been mentioned, the shifting in time of the function $f(t-\tau_s)$ is due to the exponential term in the Laplace transform of the motion input P(s) of Equation (11d). In the ramp case, f(t) has the form:

$$f(t) = A + Et + Be^{bt} + Ce^{ct} + De^{dt} + Fe^{ft} + e^{ht}(G\cos\omega_1 t + H\sin\omega_1 t) + e^{jt}(J\cos\omega_2 t + K\sin\omega_2 t) + e^{mt}(M\cos\omega_3 t + N\sin\omega_3 t) \quad (14b)$$

Notice the ramp motion gives rise to a term proportional to time t. This might be expected since the ramp motion produces an upwash at the 3/4 chord proportional to t. For times beyond τ_s, this term goes to $E\tau_s$ (=const) to give the steady state lift. The constants in f(t) and are given in the following table.

Table 3. Constants for Generalized Coordinates for Sudden Ramp Input using Wagner Function

	$q_1(t)$	$q_2(t)$	$g(t)$
A	-0.3578	-2.91e-3	-2.874e-4
B	0.3246	-1.335e-3	8.305e-7
C	1.759e-2	4.467e-3	-4.240e-7
D	8.482e-2	-4.460e-4	3.971e-6
E	9.548e-2	9.205e-4	0
F	5.894e-4	1.114e-3	1.20e-7
G	-6.988e-2	3.190e-5	1.918e-4
H	1.106e-2	-2.777e-5	-1.367e-4

J	-1.135e-4	-1.278e-3	4.527e-5
K	4.573e-4	4.463e-3	-2.046e-4
M	1.644e-4	6.946e-5	4.579e-5
N	-2.327e-3	-1.027e-3	-3.055e-3

*The values of the remaining constants are the same as given in Table 2.

The above solutions are in closed form and have the mathematical properties that might be anticipated. That is, the exponential terms giving the response to a circulatory build-up in lift after the motion input, and an oscillatory component which occurs at three distinct frequencies that arise due to the modal excitation and coupling in the forcing terms on the RHS of Equations (3). Notice the reduction in the aeroelastic frequencies in the results above from the natural frequencies (given previously) in the respective modes due to apparent mass effects. The solutions given above are plotted in Figures 5a-l where the modal coupling can be observed in the frequency content of each modal solution. The solutions are given for both the step and ramp motions and have been calculated using both the Wagner function and the Kussner function as the indicial lift. The conditions are indicated in the caption of each figure. As might be expected the step input tends to excite the higher frequency TDOF more than the more gradual ramp input.

A comparison of Figures 5g and 5h as well as Figures 5i and 5j indicates that the oscillations in the Kussner function solution persist for a longer period of time than the Wagner solution. This is due to the fact that the Kussner function provides no damping at the step onset where the Kussner function has a value of zero. The Wagner function, on the other hand, has an instantaneous value of 0.5 at the step origin which provides significant damping through the integral terms in Equations (6).

It is of course possible to input other motions than those of Equations (11a) and (11b). For example, the trigonometric function: $p(t) = (\Delta\alpha/2\pi)(\omega_s t - \sin\omega_s t)(\mu(t-0) - \mu(t-\tau_s)) + \Delta\alpha\mu(t-\tau_s)$ may be used to represent the step, where $\omega_s = 2\pi/\tau_s$. This function has continuous first and second derivatives. The solution for the generalized coordinate is of the form $f(t) - \mu(t-\tau_s) f(t-\tau_s)$, where:

$$f(t) = A + Et + (U\sin\omega_s t + V\cos\omega_s t) + Be^{-bt} + Ce^{-ct} + De^{-dt} + Fe^{-ft} + e^{-ht}(G\sin\omega_1 t + H\cos\omega_1 t) + e^{-jt}(J\sin\omega_2 t + K\cos\omega_2 t) + e^{-mt}(M\sin\omega_3 t + N\cos\omega_3 t) \quad (14c)$$

Notice that the period of ω_s is τ_s and consequently, the harmonic terms containing ω_s cancel identically for times greater than τ_s (according to $f(t) - \mu(t-\tau_s) f(t-\tau_s)$). The results for this input are similar to the ramp input and are not presented here.

Calculation of the Sensible Normal Force at the Load Cell

The purpose of the present analysis is to determine the effects of aeroelasticity on the output of the strain gauge load cell used in the experiments described above. In these experiments the strain gauge output is interpreted ideally as that due to a moment exerted by a normal force applied at the midspan of the submerged part of the airfoil (point loads were applied here to calibrate the strain gauge bridge). In reality, however, this is not the case since the strain gauge output is determined solely by the instantaneous beam curvature at the cell. This curvature is due, not to aerodynamic loading alone, but rather the total aeroelastic structural response.

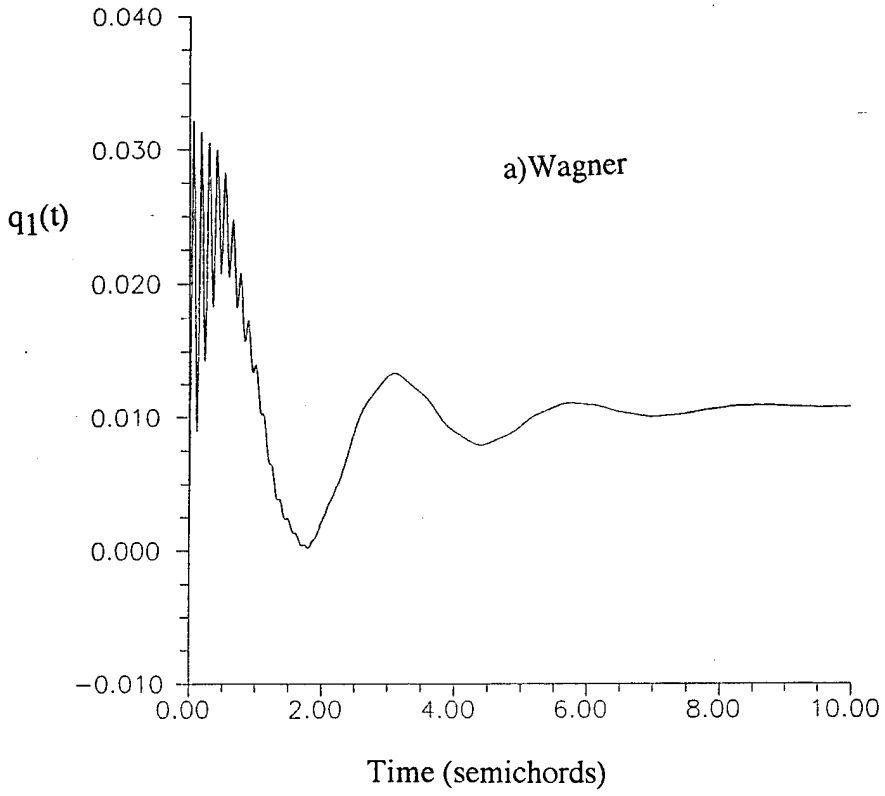

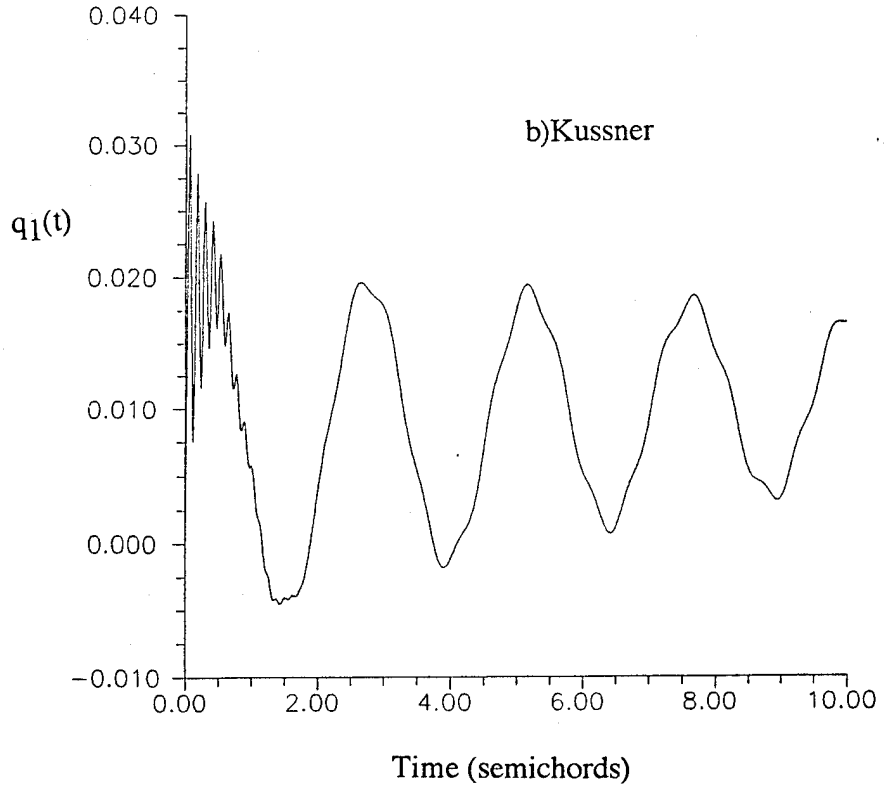

Figures 5a and 5b. Step Solution for the NDOF1 Generalized Coordinate $q_1(t)$ using: a)Wagner Function, b)Kussner Function.

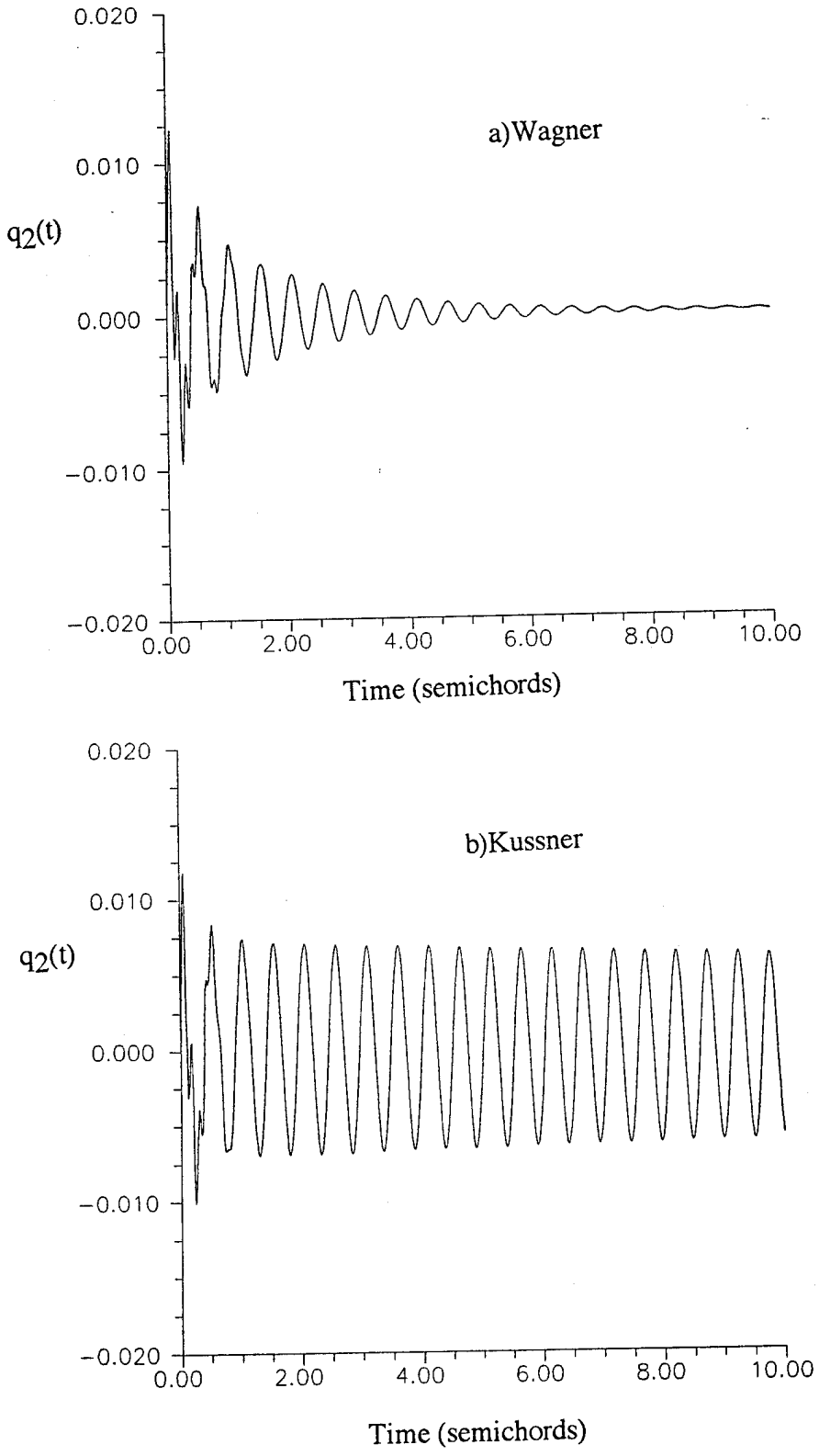

Figures 5c and 5d. Step Solution for the NDOF2 Generalized Coordinate $q_2(t)$ using: a)Wagner Function, b)Kussner Function.

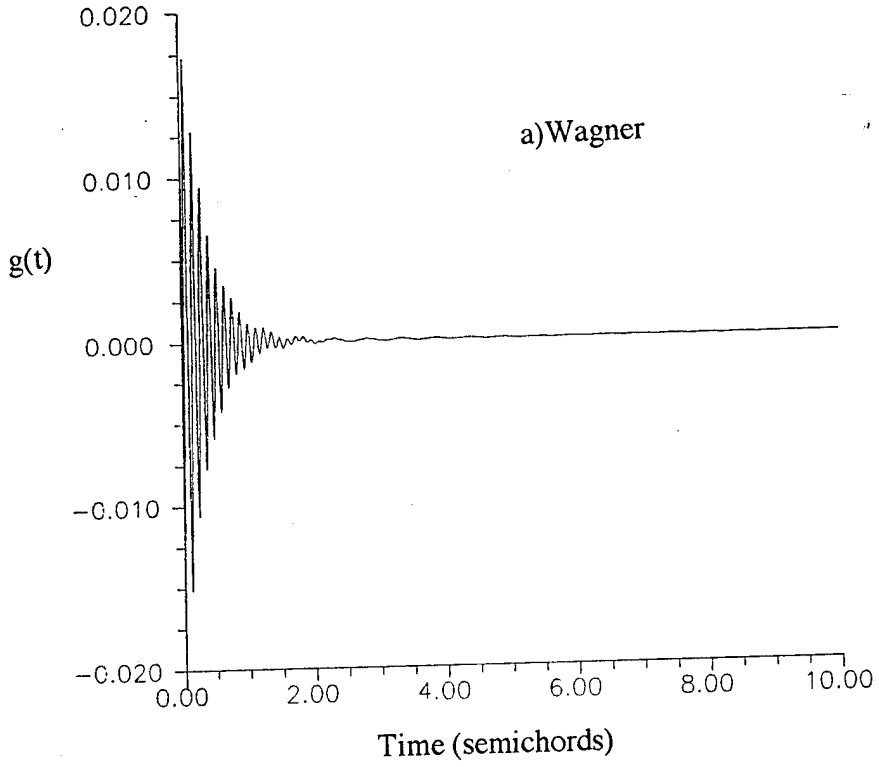

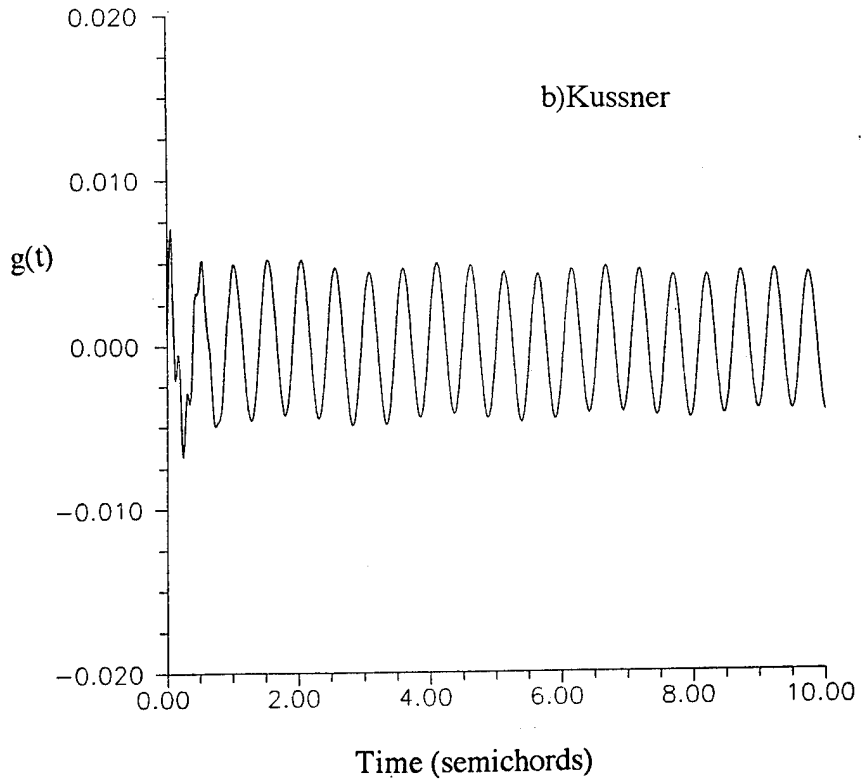

Figures 5e and 5f. Step Solution for the TDOF Generalized Coordinate g(t) using: a)Wagner Function, b)Kussner Function.

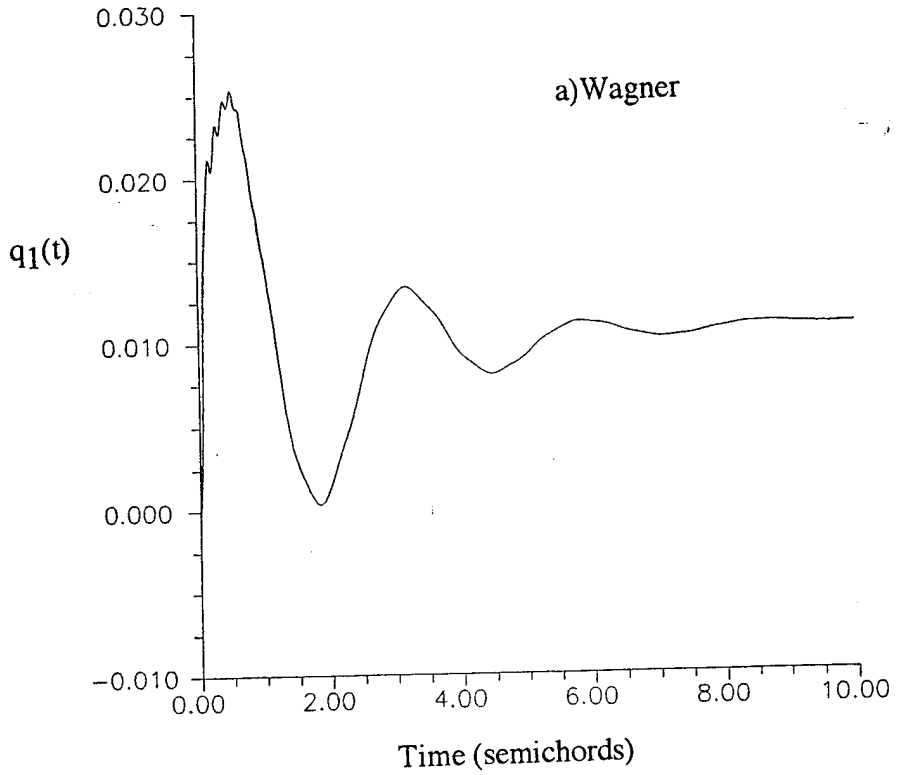

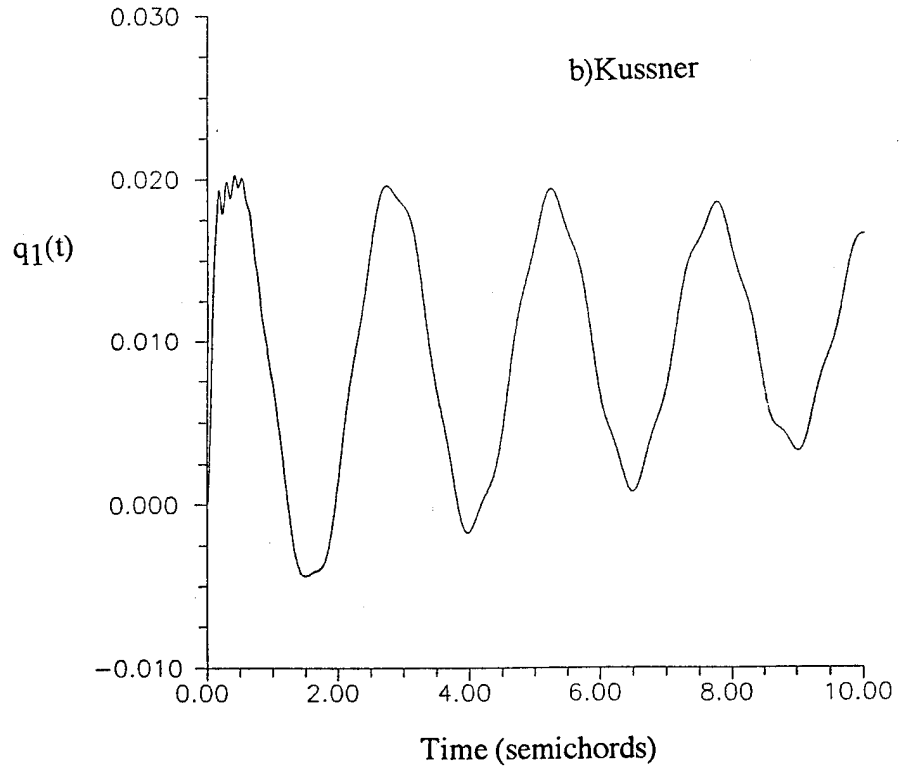

Figures 5g and 5h. Ramp Solution for the NDOF1 Generalized Coordinate $q_1(t)$ using: a)Wagner Function, b)Kussner Function.

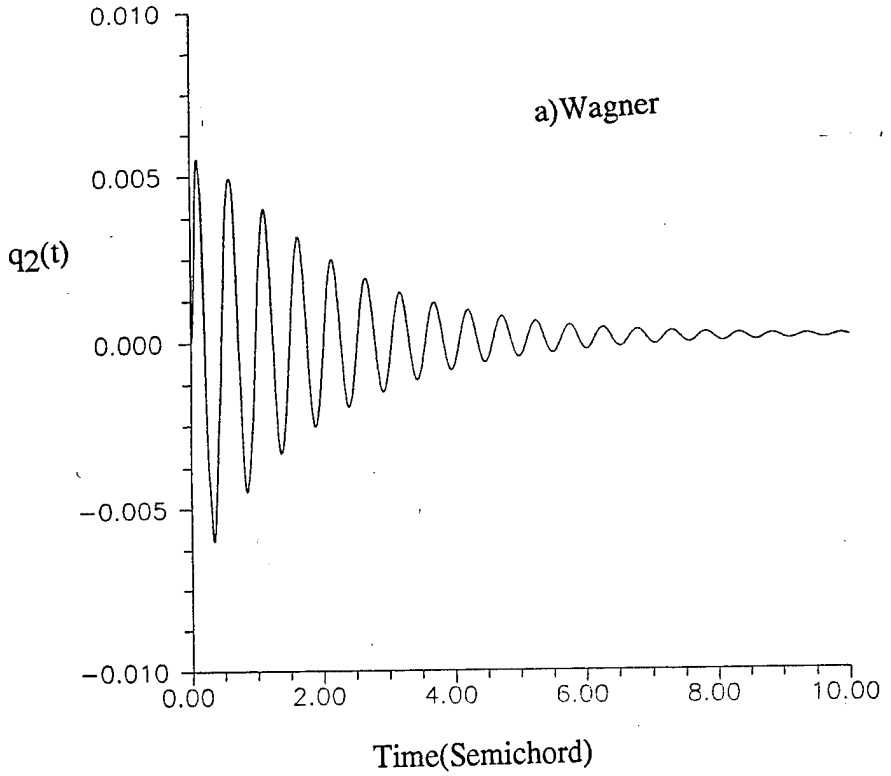

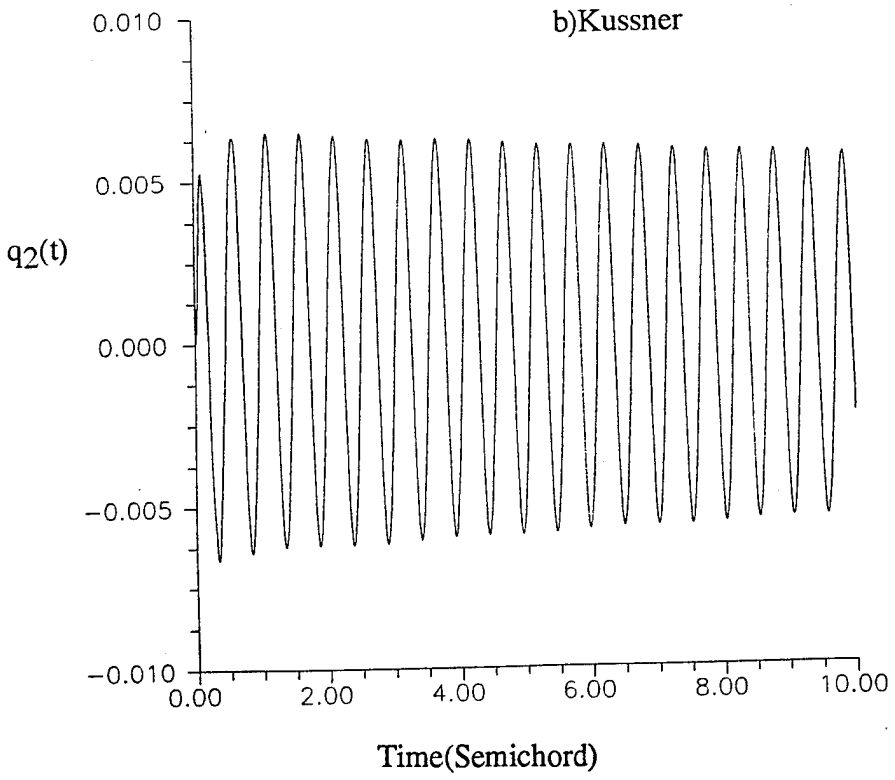

Figures 5i and 5j. Ramp Solution for the NDOF2 Generalized Coordinate $q_2(t)$ using: a)Wagner Function, b)Kussner Function.

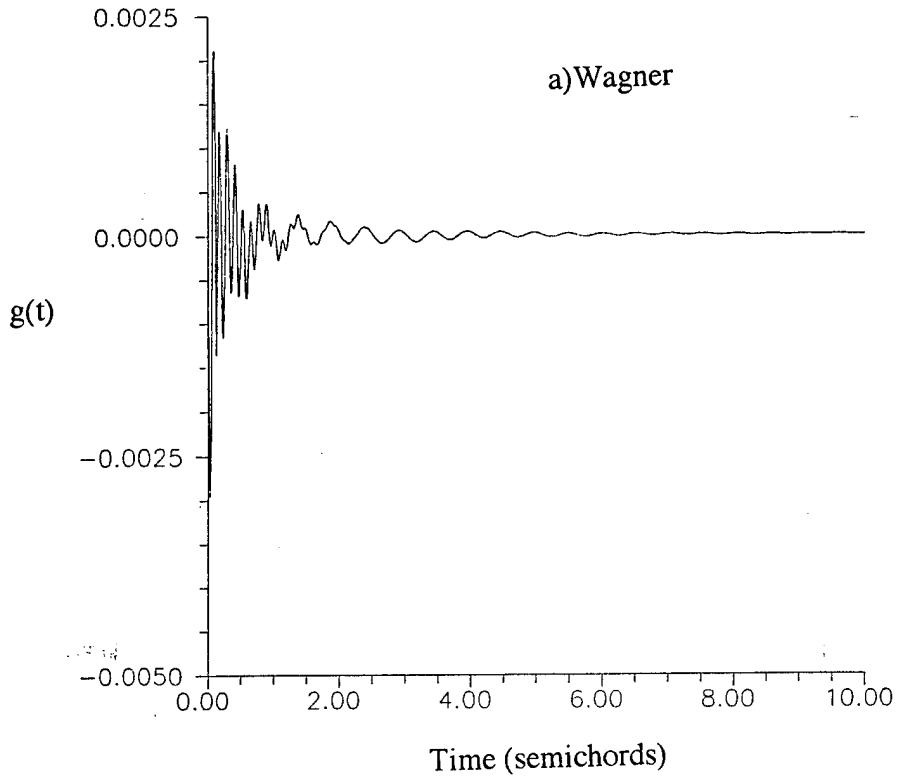

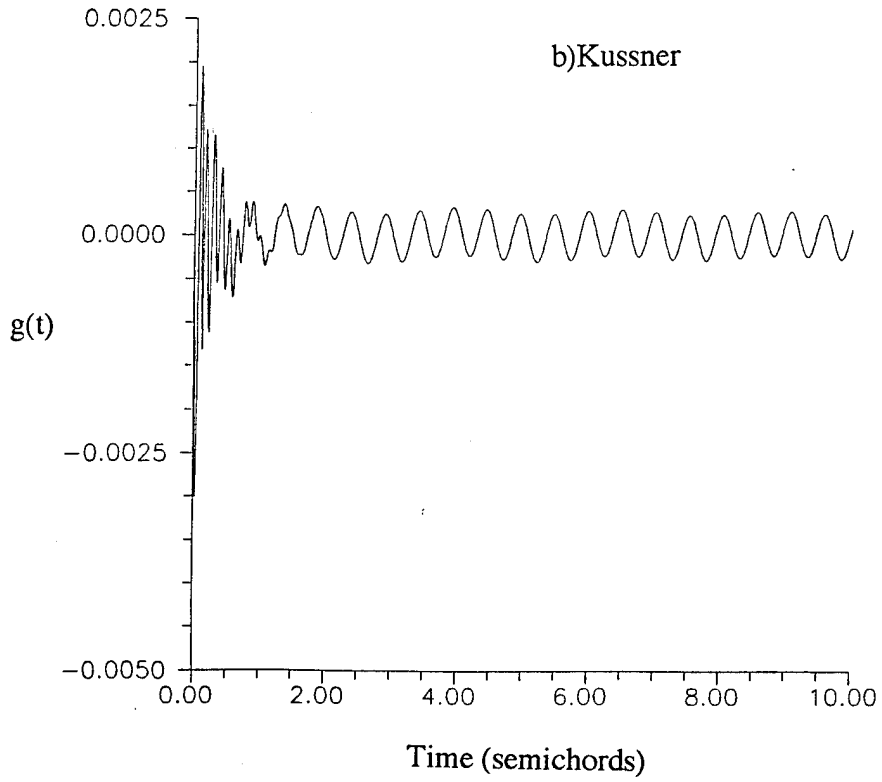

Figures 5k and 5l. Ramp Solution for the TDOF Generalized Coordinate g(t) using: a)Wagner Function, b)Kussner Function.

From beam theory the moment at the center of the load cell (centroid of element 7) is related to the beam curvature by:

$$M_{LC}(t) = EI\{q_1(t)\frac{d^2\phi_{N1}}{dx^2}\Big)_7 + q_2(t)\frac{d^2\phi_{N2}}{dx^2}\Big)_7\} \tag{15a}$$

where x is measured along the span. The second derivative has been computed numerically from the NDOF mode shapes for elements 5 through 9 using a five point numerical derivative given by Richardson's extrapolation method [10]. A time dependent "sensible" normal force acting at the midspan of the submerged portion of the airfoil which produces the same moment as that given by Equation (15a) may then be defined for comparison with experimental normal force data. For this purpose, the moment arm between the mass 7 and the midspan is $L_{LC} = 37.0$ in. These results are presented in the form of a sensible normal force coefficient defined as:

$$C_N(t) = C_{No} + \frac{M_{LC}(t)/L_{LC}}{\rho U^2 bL} \tag{15b}$$

where C_{No} is the normal force at the origin of the motion, ρ is the density of water, and L is the submerged airfoil length (42.0 in), U and b are the freestream velocity and the semichord length, respectively.

Aeroelastic Analysis Results

Sensible force calculations using the present model are compared below with the experimental normal force data of Reference [4]. A comparison is also made with recent accelerometer data taken on the Ohio U. tow tank rig undergoing the motion illustrated in Figure 2. In these tests an accelerometer (PCB Flexcel Series 336A) was placed on mass 13 (see Figure 1b) with the accelerometer centered on the pitch axis. The accelerometer data have been integrated once and put in the form of velocity. The present model can predict velocity at any point on the structure by taking the time derivative of Equations (2). The accelerometer data and normal force data below were acquired in separate runs.

Sensible Force and Accelerometer Comparisons

The two motion inputs given by Equations (11a) and (11b) have been considered. The sensible force corresponding to the step input is compared with experimental strain gauge data in Figures 6a and 6b. Figure 6a has been computed using Wagner's function and Figure 6b has been computed using Kussner's function. Also shown is the theoretical response based on the Wagner function and Kussner function, respectively. There are three frequencies present in the aeroelastic model. The lowest frequency has a period of approximately 2.5 semichords and is associated with the NDOF1 fundamental mode. The second frequency has a period of about 0.5 semichords and is due to the NDOF2 mode, and the third highest frequency with a period near 0.1 semichord is due to the coupling between the TDOF and the NDOF1 and NDOF2. It is clear that aeroelastic reactions have caused significant deviation from the theoretical response particularly before about 1.5 semichords.

The sensible force based on the aeroelastic response with the sudden ramp input of Equation (11b) is illustrated in Figures 6c and 6d. The response directly after the motion inception is in better agreement with

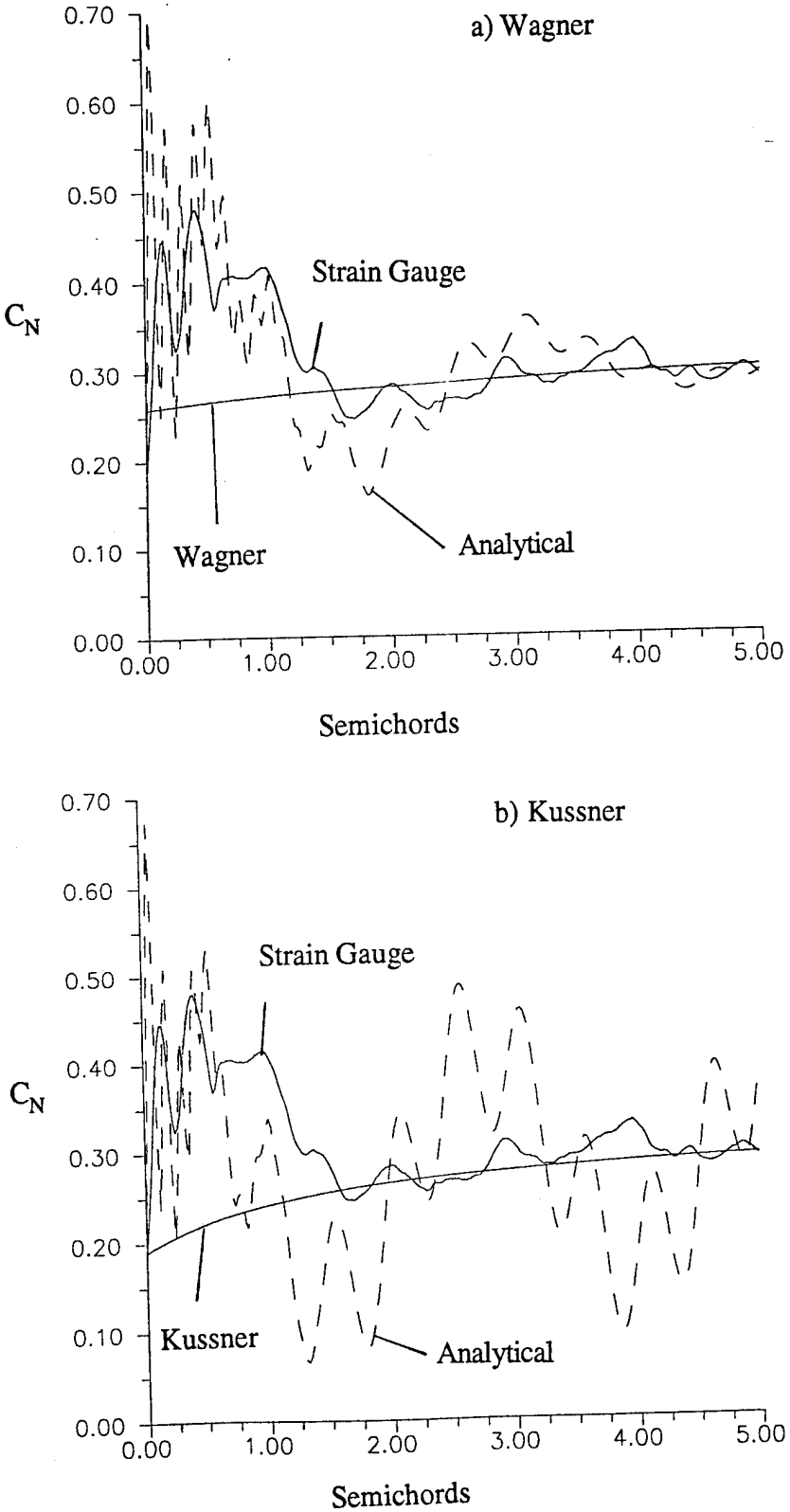

Figures 6a and 6b. Sensible Force Results for Step Input using :
a) Wagner function, b) Kussner function

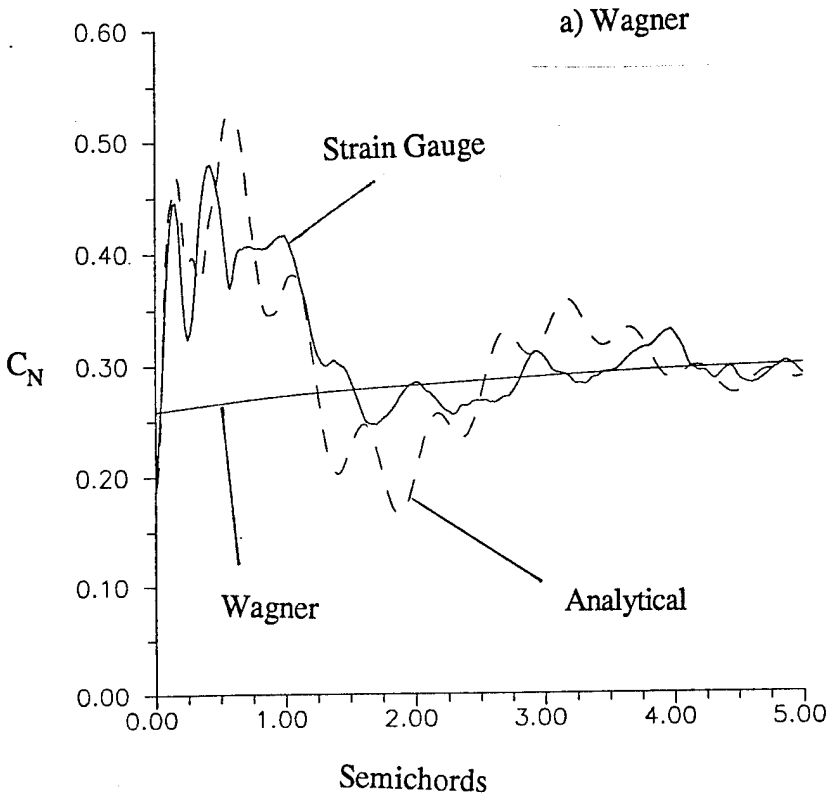

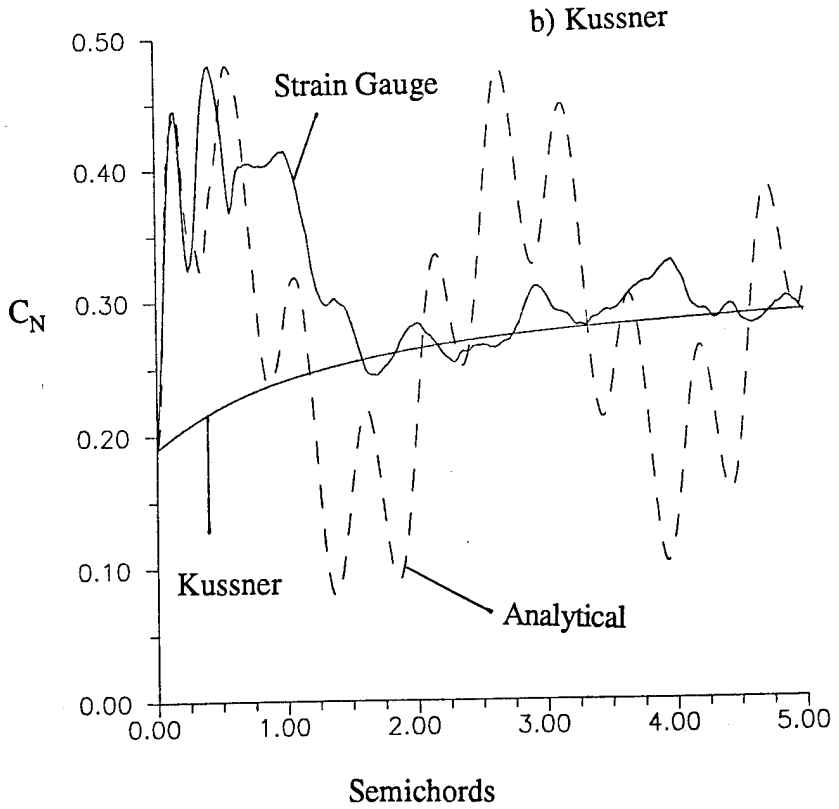

Figures 6c and 6d. Sensible Force Results for Ramp Input using :
a) Wagner function, b) Kussner function

the strain gauge data than the step input results. A comparison of the aeroelastic response of Figures 6a,b and 6c,d indicates that the step input excites the NDOF and TDOF coupling more than the sudden ramp motion. At small times the experimental data exhibit discernible oscillations, which in the analytical force, are associated with the NDOF2 mode. The amplitude of these oscillations is in better agreement with the Wagner function model than the Kussner. As has been pointed out in relation to Figures 5i and 5j, the Kussner function provides very little damping of the NDOF2 mode, which is also evident in the sensible force results of Figure 6d. It appears that the use of the Wagner function gives better agreement overall with the experimental data. It should be noted that the uncertainty in the experimental data is near 10%.

A comparison between the aeroelastic analysis using motion 1 step input and accelerometer data is shown in Figure 7a (based on Wagner function). The accelerometer data have been integrated numerically and put in the form of velocity data. Again, the use of the step function input excites the TDOF mode more than the experimental data indicates. The use of the sudden ramp motion gives the results of Figure 7b (based on Wagner function) where the agreement between the experimental data and the analysis is very good. Use of Kussner's function gives results similar to those in Figures 7a and 7b.

Part II: Inverse Aeroelastic Analysis

Described below is an inverse aeroelastic analysis directed towards computing the aerodynamic indicial response given the system structural properties and the total aeroelastic response. The aeroelastic response may be known from experimental strain gauge and/or accelerometer data which by their very nature will contain the total aeroelastic response. The following analysis focuses on computing Wagner's function from the analytical aeroelastic response which has been described in detail above. Only the ramp input motion is considered.

The problem in the inverse analysis may be stated as follows: Given the structural properties of a system(i.e. mass and stiffness) and the time dependent aeroelastic response to a known excitation (motion input), what must the aerodynamic indicial response be to produce this aeroelastic response?

Indicial Response Formulation

The Laplace transform method has been used in the present inverse analysis. Taking the Laplace transform of Equation (3a), simplifying, and rearranging yields an expression of the form:

$$\left(a_1 s + \frac{a_2}{s}\right)Q_1(s) + a_3 s Q_2(s) + (a_4 + a_5 s)(P(s) + G(s)) = [a_6 s Q_1(s) + a_7 s Q_2(s) + a_8(1 + s)(P(s) + G(s))]\gamma(s) \qquad (16)$$

where , s, is the Laplace variable, a_1 through a_8 are constants, and as before, $Q_1(s)$, $Q_2(s)$, and G(s) are the Laplace transforms of the time dependent generalized coordinates $q_1(t)$, $q_2(t)$, and g(t). The term P(s) is the Laplace transform of the ramp motion input (Equation (11d) given by: $P(s) = \frac{\Delta\alpha}{\tau_s}(1 - e^{-s\tau_s})$, $\gamma(s)$ is the Laplace transform of the indicial response function (Wagner function) which is to be determined. It should be noted that the terms in Equation (16) containing P(s) and G(s) have been grouped together. This is a due to the particular structure being modeled wherein the value of the mode shape in the TDOF is unity

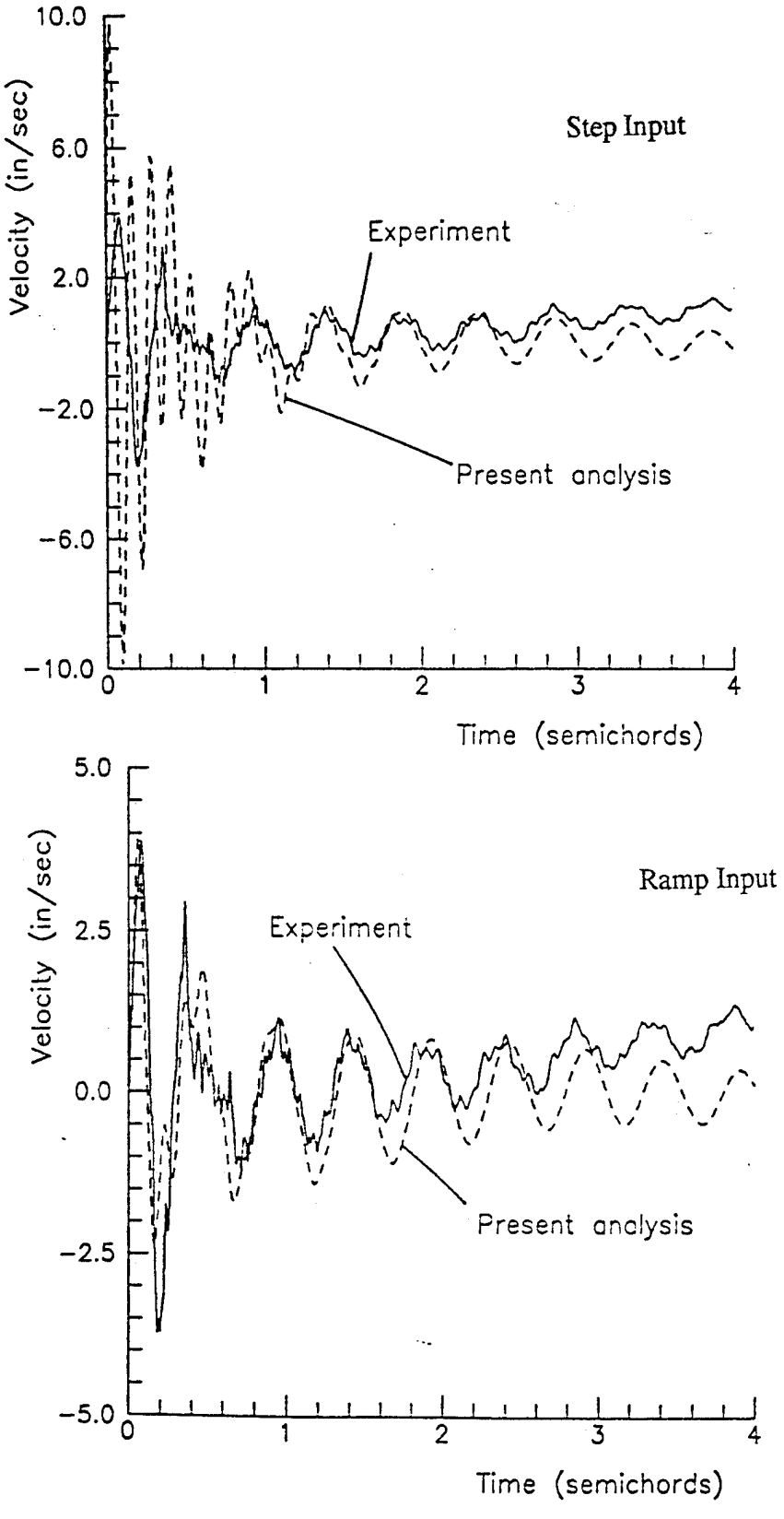

Figures 7a and 7b. Comparison of Velocity Predictions (using Wagner function) and Integrated Accelerometer Data for Step and Ramp Input Motions

for elements 13 through 23 (see Figures 1b and 3). The result is that the terms containing the RDOF coordinate P(s) and the TDOF coordinate G(s) have the same coefficients.

Equation (16) may further be simplified by eliminating the TDOF variable G(s) as follows. Taking the Laplace transform of the TDOF Equation (3c) and solving for G(s) yields an expression of the form:

$$G(s) = \left(\frac{1}{c_1 s^2 + c_2 s + c_3}\right)\left((c_4 s + c_5 s^2)P(s) + c_6 s^2 Q_1(s) + c_7 s^2 Q_2(s)\right) \tag{17}$$

where c_1 through c_7 are constants. Notice that G(s) is not a function of the indicial response $\gamma(s)$ which is a consequence of the pitch axis being located at the quarter chord. From an experimental design standpoint this is a judicious choice since it simplifies the equations of aeroelasticity. Substituting Equation (17) into (16), simplifying to eliminate any superfluous constants, and solving for the indicial function $\gamma(s)$ yields:

$$\gamma(s) = \frac{B_1(s)Q_1(s) + B_2(s)Q_2(s) + B_3(s)P(s)}{B_4(s)Q_1(s) + B_5(s)Q_2(s) + B_6(s)P(s)} \tag{18}$$

where:

$$B_1(s) = b_1 + \frac{b_2}{s^2} + \frac{s(b_3 + b_4 s)}{s^2 + b_5 s + b_6} \tag{19a}$$

$$B_2(s) = b_7 + \frac{s(b_8 + b_9 s)}{s^2 + b_5 s + b_6} \tag{19b}$$

$$B_3(s) = \frac{b_{10}}{s} + b_{11} + \frac{(b_{12} + b_{13} s + b_{14} s^2)}{s^2 + b_5 s + b_6} \tag{19c}$$

$$B_4(s) = b_{15} + \frac{b_{16} s(1+s)}{s^2 + b_5 s + b_6} \tag{19d}$$

$$B_5(s) = b_{17} + \frac{b_{18} s(1+s)}{s^2 + b_5 s + b_6} \tag{19e}$$

$$B_6(s) = b_{19}\left(1+\frac{1}{s}\right) + \frac{(b_{20} + b_{21} s + b_{22} s^2)}{s^2 + b_5 s + b_6} \tag{19f}$$

where the lower case b_1 through b_{22} are known constants, given in Appendix A. The physical origins of the constants b_1 through b_{22} may of course be traced to the constants in the Equations (3a) and (3c). For example, b_2 is the generalized stiffness K_1 in Equation (3a). Variations of Equations (19) are of course possible depending on how one chooses to perform the simplifying algebra. The forms above have been found efficacious in that, as will be seen, it will be necessary to express the Laplace variable , s, as a

complex number and then separate the resulting real and imaginary parts of the $B_1(s)$ through $B_6(s)$ functions of Equations (19).

The principal task is to perform the inverse Laplace transform of Equation (18) for known $Q_1(s)$, $Q_2(s)$, and P(s). In situations where $q_1(t)$, $q_2(t)$, and p(t) are known analytical functions of time it will generally be possible to express $Q_1(s)$, $Q_2(s)$, and P(s) as functions of s by simply taking their Laplace transforms. In this case it would theoretically be possible to substitute the transformed functions into Equation (18) and invert the resulting expression for $\gamma(s)$ analytically using partial fraction decomposition. This is essentially the approach that has been used in the aeroelastic analysis described in the Part I of this report, where the transformed indicial function $\gamma(s)$ has been expressed in analytical form and the resulting expressions for $Q_1(s)$, $Q_2(s)$, and G(s) have been inverted analytically for a given motion input P(s).

It is a purpose of this research to investigate a method for experimentally determining the indicial function and, as such, it is expected that the functions $q_1(t)$, $q_2(t)$, and the motion input p(t) will be in the form of discrete data in time which generally cannot be curve fit with simple closed form functions. As will be seen, in this instance it is possible to perform a numerical Laplace inversion of Equation (18). As discussed below, the functions $q_1(t)$ and $q_2(t)$ may be obtained from the total aeroelastic response contained in strain gauge and/or accelerometer data.

In the above analysis Equation (3a) (NDOF1) and (3c) (TDOF) have been combined to give Equation (18). It is alternatively possible to use Equations (3b) (NDOF2) and (3c), however, it has been found that the use of (3a) rather than (3b) is a more robust formulation. Although no systematic error analysis has been performed, it appears that determining (from experimental data) the NDOF2 coordinate, $q_2(t)$, is more susceptible to error than determination of the larger NDOF1 coordinate, $q_1(t)$. Equation (3a) is less sensitive to these errors than Equation (3b) since the coefficients of $q_2(t)$ in (3a) are an order of magnitude smaller than those in (3b). It is also possible to combine all three Equations (3a), (3b), and (3c). This method has likewise been found to be less stable than that based on Equations (3a) and (3c).

Numerical Inverse of Laplace Transform

The method of Reference[11] has been used to numerically invert Equation (18). Briefly, the method evaluates the inverse by means of a Fourier series, and is essentially a numerical computation of the Laplace inversion formula:

$$\Gamma(t) = \frac{1}{2\pi i} \int_{a-i\infty}^{a+i\infty} e^{st}\, \gamma(s)\, ds \qquad (20)$$

where , a, is a constant such that any singularities of $\gamma(s)$ lie to the left of the line integral in the complex plane. Letting $s = a + i\omega$ so that $\gamma(s) = \gamma(a,\omega)$, Equation (20) may alternatively be expressed by:

$$\Gamma(t) = \frac{e^{at}}{\pi} \int_0^{\infty} [\, \mathrm{Re}\,(\gamma(a,\omega))\cos\omega t - \mathrm{Im}\,(\gamma(a,\omega))\sin\omega t\,]\, d\omega \qquad (21)$$

A trapezoidal rule approximation to Equation (21) on the time interval (0,2T) is given by:

$$\Gamma(t) = \left(\frac{e^{at}}{T}\right)\left[\frac{\gamma(a)}{2} + \sum_{k=1}^{\infty}\left\{ \mathrm{Re}\left(\gamma\ (a\ ,\ k\pi/T)\right)\cos(k\pi t/T) - \mathrm{Im}\left(\gamma\ (a\ ,\ k\pi/T)\right)\sin(k\pi t/T)\right\}\right] \qquad (22)$$

Equation (22) provides an approximation to the exact value of the indicial response function. The value of T is chosen to be $T = 0.8\ t_{max}$, where t_{max} is the largest time for which $\Gamma(t)$ is to be approximated. The value of a is chosen according to $a = \alpha - \ln(E)/2T$, where α is a number slightly larger than the maximum real pole of $\gamma(s)$, and E is the desired maximum relative error. The relative error is defined as the error in the approximation divided by the maximum value of the function to be approximated. Thus, if the approximation is to converge to at least two significant figures the relative error would be set to 0.005. Of course in practice the summation in Equation (22) would contain only a finite number of terms designated henceforth as N. The reader may consult Reference [11] for additional details of the inversion method.

To numerically invert Equation (18) using Equation (22), it is necessary to treat the Laplace variable, s, as a complex number and separate $\gamma(s)$ into real and imaginary parts. The functions $B_1(s)$ through $B_6(s)$ as well as the transformed generalized coordinates $Q_1(s)$ and $Q_2(s)$ and the motion input P(s) will each contain a real and imaginary part. Letting $s = x + iy$, the resulting expression for $\gamma(s)$ will be given by:

$$\gamma(x,y) = \gamma_R(x,y) + i\,\gamma_I(x,y) \qquad (23a)$$

where $\gamma_R(x,y)$ and $\gamma_I(x,y)$ are the real and imaginary parts, respectively, of $\gamma(x,y)$ which are given by:

$$\gamma_R(x,y) = \frac{N_R S_R + N_I S_I}{S_R^2 + S_I^2} \quad , \quad \gamma_I(x,y) = \frac{N_I S_R - N_R S_I}{S_R^2 + S_I^2} \qquad (23b)$$

and:

$$N_R(x,y) = (B_{1R}Q_{1R} - B_{1I}Q_{1I}) + (B_{2R}Q_{2R} - B_{2I}Q_{2I}) + (B_{3R}P_R - B_{3I}P_I) \qquad (23c)$$

$$N_I(x,y) = (B_{1R}Q_{1I} + B_{1I}Q_{1R}) + (B_{2R}Q_{2I} + B_{2I}Q_{2R}) + (B_{3R}P_I + B_{3I}P_R) \qquad (23d)$$

$$S_R(x,y) = (B_{4R}Q_{1R} - B_{4I}Q_{1I}) + (B_{5R}Q_{2R} - B_{5I}Q_{2I}) + (B_{6R}P_R - B_{6I}P_I) \qquad (23e)$$

$$S_I(x,y) = (B_{4R}Q_{1I} + B_{4I}Q_{1R}) + (B_{5R}Q_{2I} + B_{5I}Q_{2R}) + (B_{6R}P_I + B_{6I}P_R) \qquad (23f)$$

where the subscripts R and I indicate real and imaginary parts, respectively. The separation of the generalized coordinates and the motion input into real and imaginary parts is discussed below. The separation of the functions $B_1(s)$ through $B_6(s)$ is accomplished by substituting $s = x + iy$ into the Equations (19) and performing the necessary algebra. For example, the function $B_3(x,y) = B_{3R}(x,y) + iB_{3I}(x,y)$, has real and imaginary parts given by:

$$B_{3R}(x,y) = \frac{b_{10}x}{x^2+y^2} + b_{11} + \frac{(x^2-y^2+b_5x+b_6)(b_{12}+b_{13}x+b_{14}(x^2-y^2)) + (2xy+b_5y)(b_{13}y+2b_{14}xy)}{(x^2-y^2+b_5x+b_6)^2 + (2xy+b_5y)^2} \tag{24}$$

$$B_{3I}(x,y) = \frac{-b_{10}y}{x^2+y^2} + \frac{(x^2-y^2+b_5x+b_6)(b_{13}y+2b_{14}xy) - (2xy+b_5y)(b_{12}+b_{13}x+b_{14}(x^2-y^2))}{(x^2-y^2+b_5x+b_6)^2 + (2xy+b_5y)^2}$$

The remaining expressions for $B_1(s)$ through $B_6(s)$ may similarly be separated into real and imaginary parts. For using Equation (24) in the approximating Equation (22) one would set x = a , and y = $k\pi t/T$. It should be noted that at points of discontinuity, the above method will converge to $\Gamma(t) = (\Gamma(t+) + \Gamma(t-))/2$, where t is the time of the discontinuity. Indicial responses may contain points of discontinuity such as Wagner's function which is discontinuous at t = 0.

Other numerical inversion methods may also be used such as that described in Reference [12], in which the inverse is obtained in terms of orthonormal Laguerre polynomials. The inverse transform is given by:

$$\Gamma(t) = e^{at} \sum_{n=0}^{N} c_n \Phi_n(\frac{t}{T}) \tag{25}$$

where , a, is a real constant larger than any real singularities of $\gamma(s)$, and $\Phi_n(\frac{t}{T})$ are Laguerre polynomials. The constant T is a scaling factor chosen according to: $T = t_{max}/N$, where t_{max} defines the time interval of interest, and N is the number of terms in the summation of Equation (25). This choice of T ensures that the oscillatory frequencies of the Laguerre polynomials are compatible with those of the function to be approximated. The constants c_n are given by:

$$c_o = \frac{1}{N+1} \sum_{j=0}^{N} h(\theta_j) \quad , \quad c_n = \frac{2}{N+1} \sum_{j=0}^{N} h(\theta_j) \cos(n\theta_j) \quad , n \neq 0 \tag{26a}$$

where: $$\theta_j = (\frac{2j+1}{2N+1}) \frac{\pi}{2} \qquad j = 1, 2, \ldots N \tag{26b}$$

$$h(\theta_j) = \frac{1}{2T} [\gamma_R(a, \frac{1}{2T}\cot\frac{\theta_j}{2}) - (\frac{1}{2T}\cot\frac{\theta_j}{2}) \gamma_I (a, \frac{1}{2T}\cot\frac{\theta_j}{2})] \tag{26c}$$

where $\gamma_R(x,y)$ and $\gamma_I(x,y)$ are defined above. In evaluating Equation (25) using Equations (26a)-(26c) one would set x = a, and $y = \frac{1}{2T}\cot\frac{\theta_j}{2}$. The Laguerre polynomials in Equation (25) may be evaluated using the recursion formulas:

$$\Phi_o(t) = e^{-t/2}$$
$$\Phi_1(t) = (1 - t)\Phi_o(t) \tag{26d}$$

$$n\Phi_n(t) = (2n - 1 - t)\Phi_{n-1}(t) - (n - 1)\Phi_{n-2}(t) \quad , \quad n>1$$

It has been found that this method agrees with the method of Reference [12] for intermediate and large values of time, however, for small time the method gives oscillatory results. Results from both methods are presented below.

Transform of Generalized Coordinates: Analytical Form

The numerical inversion of Equation (18) has been done using the analytical solutions for $q_1(t)$,$q_2(t)$, and g(t) given by Equation (14b) for the ramp motion input case. In this case the functions $Q_1(s)$ and $Q_2(s)$ are in the form: $F(s)\ (1 - e^{-s\tau_s})$, where F(s) is the transform of f(t) in Equation (14b). Notice from Equation (11d) that the function P(s) also contains the term $(1 - e^{-s\tau_s})$ so that in Equation (18) this term can be canceled out of numerator and denominator. For evaluating Equations (23), $Q_1(s)$ and $Q_2(s)$ may be obtained by taking the Laplace transform of Equation (14b), substituting $s = x + iy$, and separating into real and imaginary parts to obtain $Q_{1R}(x,y)$, $Q_{1I}(x,y)$,$Q_{2R}(x,y)$ and $Q_{2I}(x,y)$. The resulting expressions are rather long and are omitted here. The functions $P_R(x,y)$ and $P_I(x,y)$ are likewise obtained from Equation (11d). The software MACSYMA may be useful in performing the complex algebra.

Indicial Response Results: Analytic Form

The indicial response results are shown in Figure 8a using the method of Reference [11] along with Wagner's function. In the caption, α is a variable used to calculate the real value, a, of the Laplace variable of integration, N is the number of terms in the Fourier series, t_{max} is the largest time for which the indicial response is the approximated, and E is the relative error also used to calculate the parameter, a. Each of these quantities is a required input. It has been found that these parameters can be varied significantly and still provide good agreement with the theoretical value. For example setting N=100, t_{max}=50 , and E=.0001 yields virtually the same results. It is of course necessary to choose α to be larger than the largest real pole of $\gamma(s)$. The indicial response is underpredicted at the point of discontinuity at t=0 by one-half the actual value which, as has been mentioned, is implicit to the method. For times above about one semichord the agreement between the numerical results and the Wagner function is excellent. The oscillations in the numerical results arise from the harmonic series used in the approximation. Shown in Figure 8b are the results using the inversion method of Reference [12]. Shown in the caption is the required input to the algorithm. The method gives highly oscillatory results at small times. In fact, the data below about 0.2 semichords have been clipped because the amplitude of oscillation is off the scale of the Figure. For larger times the agreement is very good. These and subsequent calculations have been done on an IBM p.c. (Pentium) using BASIC and requires approximately 5 minutes of computation time. The calculations of the results of Figures 8a and 8b require approximately thirty seconds.

Transform of Generalized Coordinates: Discrete Form

The treatment of $q_1(t)$, $q_2(t)$, and p(t) in the form of discrete data points is directed towards the situation wherein these values would result from experimental measurements as described below. The functions for

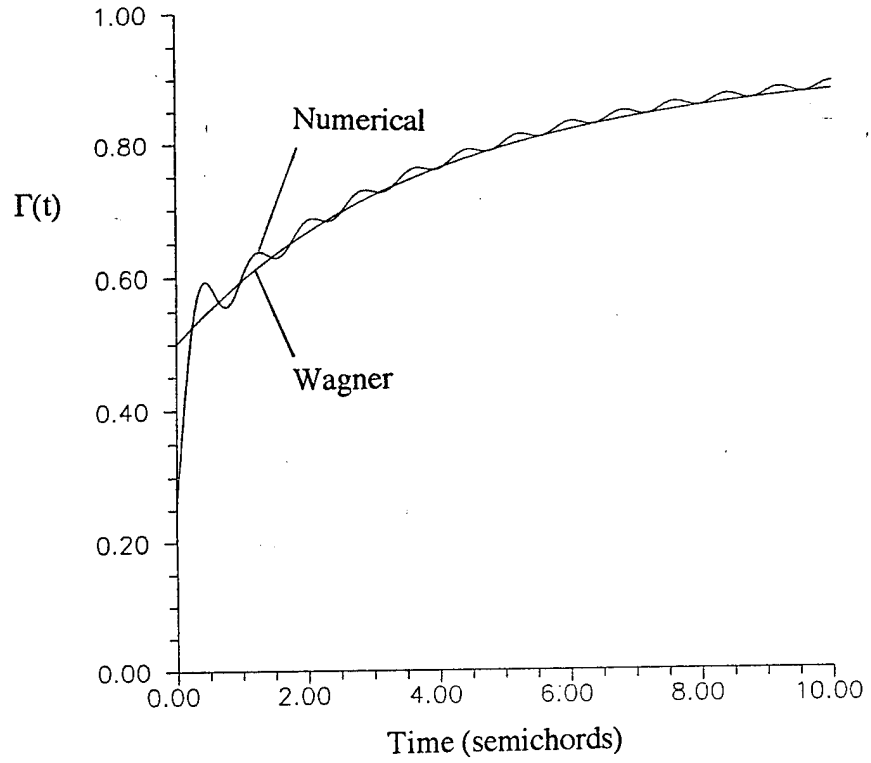

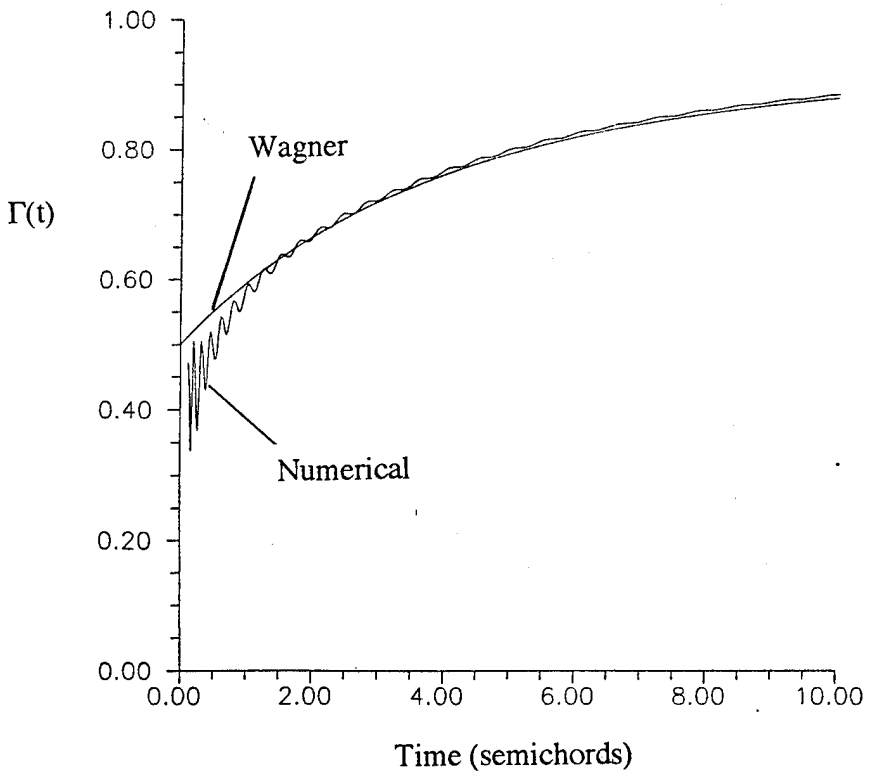

Figure 8a and 8b. Indicial Response Results for Analytical Input using 8a) Ref.[11], α=0.01, N=200, E=1e-6, t_{max}=100, 8b)Ref.[12], a=0.01, N=200, t_{max}=50.

$q_1(t)$ and $q_2(t)$ given by Equation (14b) and p(t) given by Equation (11b) have been used to generate discrete values for these functions at a time interval of $\Delta t = 0.01$ semichords (.0012 sec). This time interval was chosen because it is representative of the Ohio U. tow tank. These data when plotted would then closely resemble the curves in Figures 4, 5c, and 5e. The Laplace transform of any function f(t) is defined by:

$$F(s) = \int_0^\infty e^{-st} f(t)\, dt \tag{27}$$

If f(t) is in the form of N discrete data points f_0 , f_1 , ... f_N at times t_0 , t_1 , ... t_N , respectively, a trapezoidal rule approximation to (27) is:

$$F(s) = \Delta t \left[\frac{1}{2}(f_0 + e^{-st_N} f_N) + \sum_{j=1}^{N-1} e^{-st_j} f_j \right] \tag{28}$$

Substituting $s = x + iy$ and separating into real and imaginary parts yields $F(x,y) = F_R(x,y) + iF_I(x,y)$, where:

$$F_R(x,y) = \Delta t \left[\frac{1}{2}(f_0 + e^{-xt_N} \cos(yt_N) f_N) + \sum_{j=1}^{N-1} e^{-xt_j} \cos (yt_j) f_j \right]$$

$$F_I(x,y) = \Delta t \left[-\frac{1}{2} e^{-xt_N} \sin(yt_N) f_N) - \sum_{j=1}^{N-1} e^{-xt_j} \sin (yt_j) f_j \right] \tag{28a}$$

where the identity $e^{-iyt} = \cos(yt) - i \sin(yt)$ has been used. For evaluating Equations (28a) using the method of Reference [11] (Equation (22))one would set $x = a$, and $y = k\pi t/T$, whereas using the method of Reference [12] (Equation (26c)) $x = a$, and $y = \frac{1}{2T} \cot \frac{\theta_j}{2}$. It has been found in the present case that applying Equations (28a) over a time interval of approximately twenty semichords gives an adequate approximation to the Laplace transforms of $Q_{1R}(x,y)$, $Q_{1I}(x,y)$,$Q_{2R}(x,y)$, $Q_{2I}(x,y)$, $P_R(x,y)$ and $P_I(x,y)$.

Indicial Response Results: Discrete Form

The inverse results using method of Reference [11] is shown in Figures 9a and 9b, where it is seen that the agreement with the Wagner function is very good. A comparison of Figure 9a and 9b shows the effect of the number of terms used in the Fourier series, with the increase in the number of terms increasing the frequency content of the results. Figure 9c shows the results using the inversion routine of Reference [12] where again there are significant oscillations near the origin.

Inverse Formulation in Terms of Experimental Data

Typical experimental data may include force measurements and/or accelerometer measurements. The force measurements could be either strain gauge or integrated pressure measurements. Below we assume the existence of a set of discrete strain gauge normal force data $C_N(t)$ and a concurrent set of chord normal

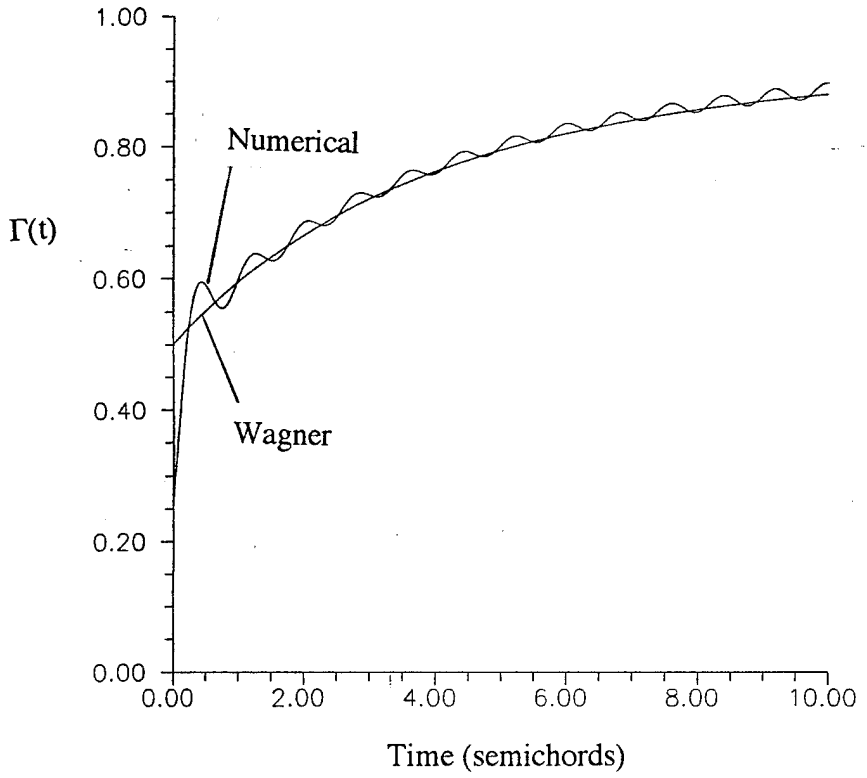

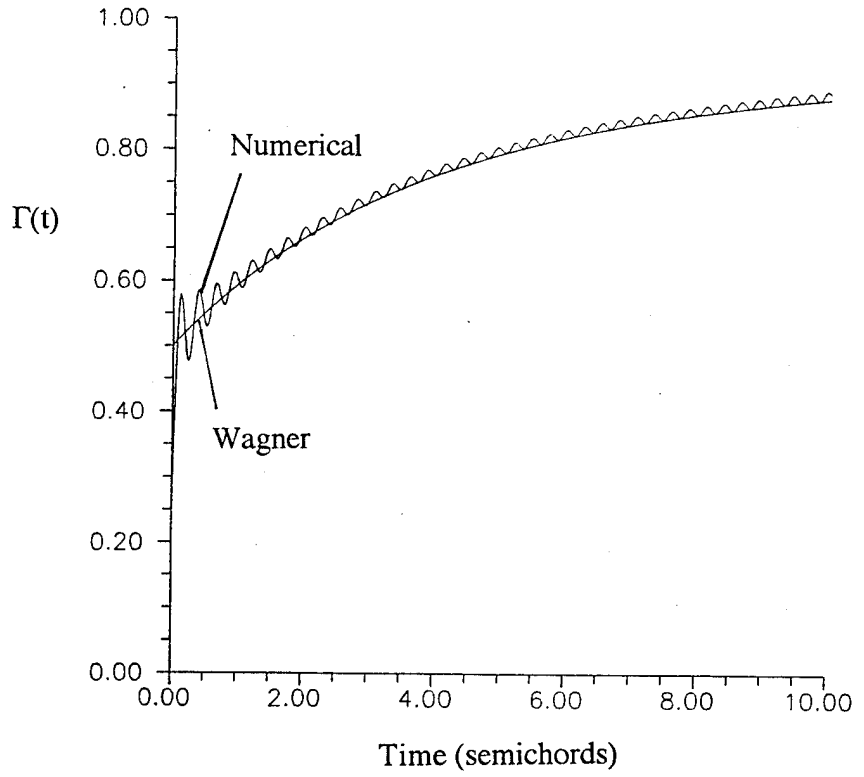

Figure 9a and 9b. Indicial Response Results for Discrete $q_1(t)$, $q_2(t)$, and p(t) Input using 9a) Ref.[11], α=0.01, N=100, E=1e-6, t_{max}=100, 9b)Ref.[11], a=0.01, N=300, t_{max}=50.

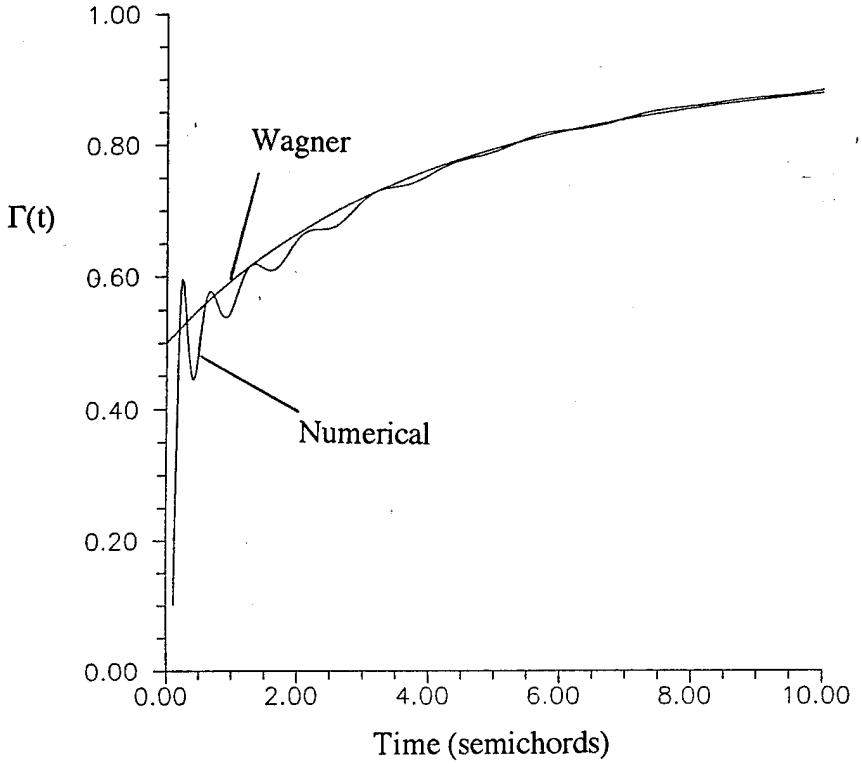

Figure 9c. Indicial Response Results for Discrete $q_1(t)$, $q_2(t)$, and p(t) Input using Ref.[12], α=0.0, N=100, t_{max}=50.

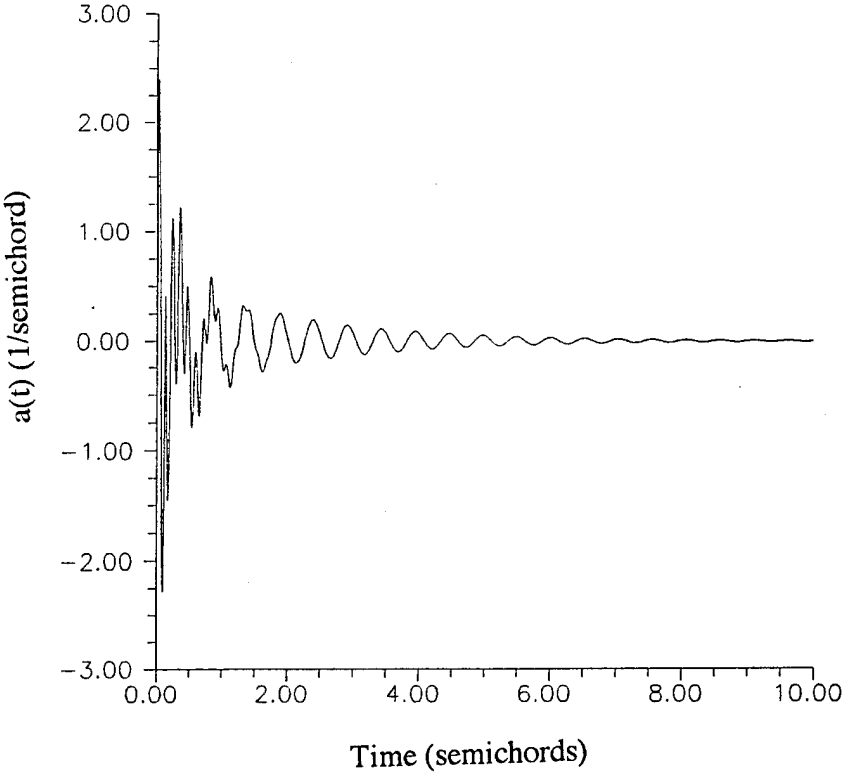

Figure 10. Analytical Acceleration Data of Element 13.

accelerometer data a(t) at some point on the structure. To initially investigate the use of experimental data, while also making use of the analytical information above for guidance, we generate fictitious normal force data and accelerometer data. The strain gauge data are the sensible force data shown previously Figure 6c (labeled "Analytical") and given by Equations (15a) and (15b). The accelerometer data are shown in Figure 10 and have been generated using:

$$a(t) = D_1\ddot{q}_1(t) + D_2\ddot{q}_2(t) \tag{29a}$$

where D_1 and D_2 are simply the values of the first and second mode shapes, respectively, at the point on the structure at which the acceleration is measured, and the derivatives of $q_1(t)$ and $q_2(t)$ are obtained by differentiating Equation (14b). The acceleration data is chosen to be the chord normal acceleration of element 13 measured on the pitch axis (see Figure 1b). The force and the accelerometer data have been generated at a time interval between data points of 0.01 semichords (.0012 sec), which is reasonable from an experimental standpoint. Note that the analytical displacement of any point on the structure is also known from the solution given by Equation (14b).

The displacement of the structure, d(t), may theoretically be obtained by numerically integrating the accelerometer data. This has been done using both a trapezoidal method as well as Simpsons three point method. Both methods have proven to give unsatisfactory results in that the error in the integrated results grows continuously as shown in Figure 11a along with the analytical displacement for comparison. The time step between data points was reduced to 0.005 with the same result. No systematic attempts have been made to pinpoint the source of the error.

The displacement may alternatively be computed from the accelerometer data by numerically solving the second order differential equation:

$$\ddot{d}(t) = a(t) \tag{29b}$$

subject to the boundary conditions $d(0) = 0$, $d(t_M) = d_{ss}$, where t_M is some time at which steady state is assumed to exist, and d_{ss} is the steady state displacement. Notice that the steady state displacement can be computed from the steady state values of $q_1(t)$ and $q_2(t)$ and their respective mode shapes without regard to actually solving Equations (3). The steady value of $q_1(t)$ can be computed directly from Equation (3a) and Equation (5). The only term on the LHS of Equation (3a) which survives in the steady state is the stiffness term, whereas on the RHS the only surviving term is the leading term in the integral of Equation (5) which becomes $C_{N\alpha}L_i\, p_{ss}$, where p_{ss} is the steady value of $p(\tau)$. The steady state value of $q_1(t)$ may be easily found from these two surviving terms. The steady value of $q_2(t)$ may likewise be found from Equation (3b). Thus, it is reasonable to assume that d_{ss} may be known a priori.

Equation (29b) has been solved using a fourth order Runge-Kutta method [10] and the results are shown in Figure 11b with the analytical displacement for comparison. The slight discrepancy between the two is in part due to the assumption of steady state after 25 semichords in the numerical results, while the analytical steady state is reached assymtotically. An advantage of the Runge-Kutta method is that it forces

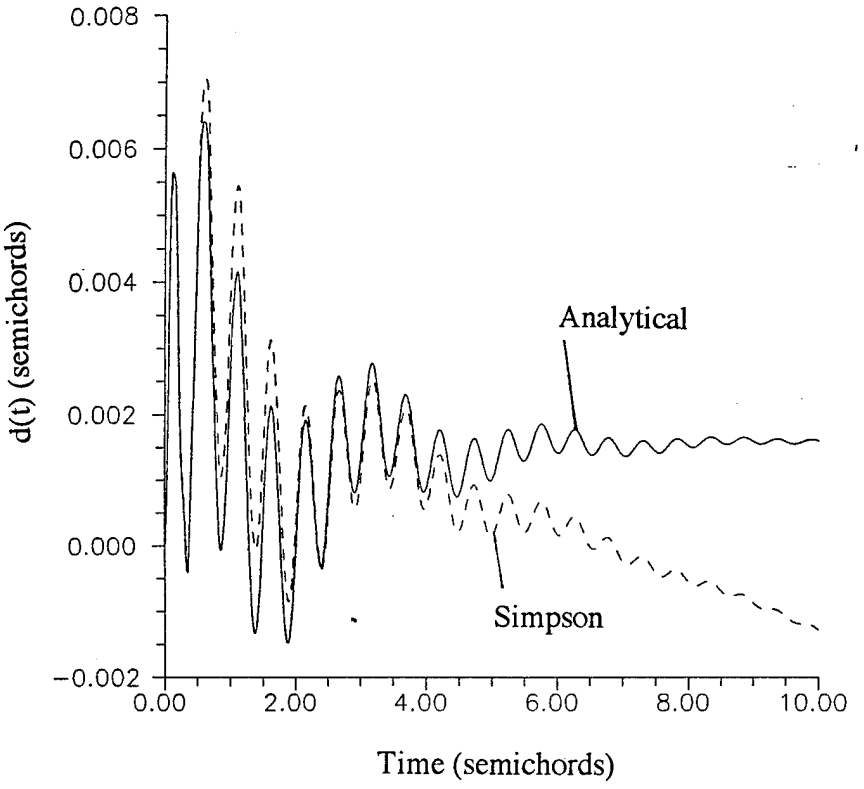

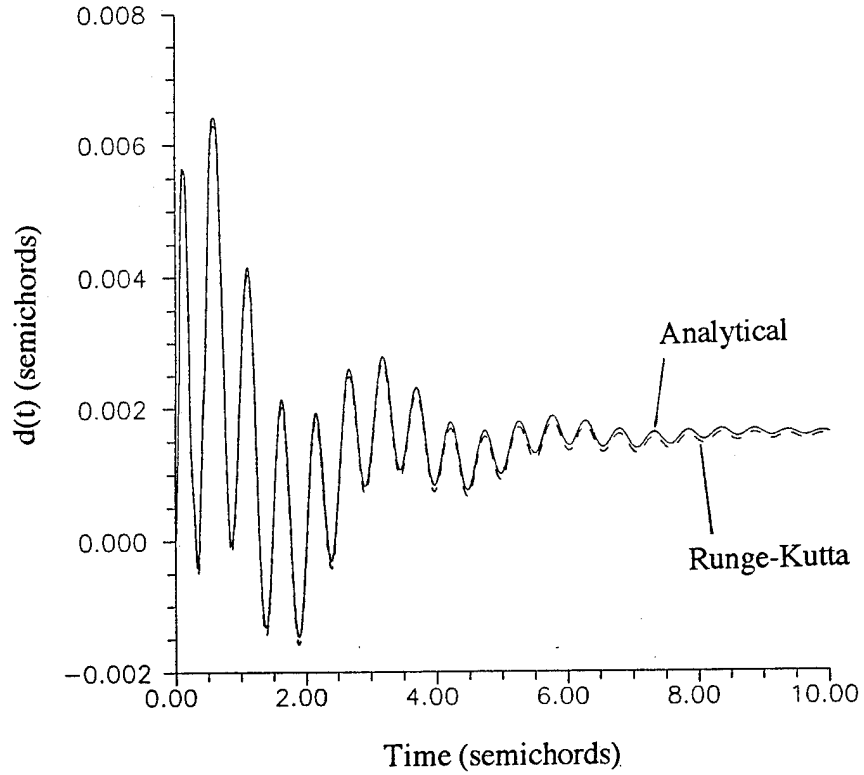

Figures 11a and 11b. Displacement Results using 11a) Simpsons Method, 11b) Fourth Order Runge-Kutta Method.

the experimental displacement to the proper steady state.

The normal force data, $C_N(t)$, and displacement data are related to the generalized coordinates by:

$$C_N(t) = K_1 q_1(t) + K_2 q_2(t) \tag{29c}$$

$$d(t) = D_1 q_1(t) + D_2 q_2(t) \tag{29d}$$

where the constants K_1 (=12.014) and K_2 (=5.148) can be deduced from Equations (15a) and (15b). Taking the Laplace transform, letting $s = x + iy$, and solving for the real and imaginary parts of Q_{1R}, Q_{1I}, Q_{2R}, and Q_{2I} yields:

$$Q_{1R}(x,y) = (D_2 C_{NR}(x,y) - K_2 D_R(x,y))/(D_2 K_1 - D_1 K_2) \tag{30a}$$

$$Q_{1I}(x,y) = (D_2 C_{NI}(x,y) - K_2 D_I(x,y))/(D_2 K_1 - D_1 K_2) \tag{30b}$$

$$Q_{2R}(x,y) = (C_{NR}(x,y) - K_1 Q_{1R}(x,y))/K_2 \tag{30c}$$

$$Q_{2I}(x,y) = (C_{NI}(x,y) - K_1 Q_{1I}(x,y))/K_2 \tag{30d}$$

where $C_{NR}(x,y)$ and $C_{NI}(x,y)$ are the real and imaginary parts, respectively, of the transformed normal force data, and $D_R(x,y)$ and $D_I(x,y)$ the real and imaginary parts of the displacement data, both pairs being evaluated numerically using Equations (28a). Equations (30) provide the relations for the generalized coordinates necessary to evaluate Equations (23). Figure 12 is a flow chart of the procedure for using the experimental data in the inversion routine of Reference [11].

It should be noted that theoretically it is possible to arrive at the transforms of the generalized coordinates directly from the accelerometer data without solving Equation (29b) to obtain displacement. The Laplace transform of Equation (29a) is:

$$A(s) = s^2(D_1 Q_1(s) + D_2 Q_2(s)) \tag{31}$$

where A(s) is the Laplace transform of a(t). Setting $s = x + iy$, Equation (31) may be combined with Equation (29c) to provide alternative relations for Q_{1R}, Q_{1I}, Q_{2R}, and Q_{2I} in terms of $C_{NR}(x,y)$, $C_{NI}(x,y)$, and $A_R(x,y)$, $A_I(x,y)$ where, as before, these quantities are evaluated using Equations (28a). This method has proven unsuccessful since Equation (28a) is a trapezoidal rule integration and as has been seen (Figure 11a), integration of the acceleration data by this method is unstable.

Inverse Indicial Response Results: Experimental Data Formulation

The inverse results using the fictitious strain gauge and displacement data are shown in Figure 13. These results are based on the method of Reference [11]. The numerical results are slightly larger than the theoretical indicial response. This difference may be attributed to error introduced in the calculation of the

I. Input: Necessary Constants

Input: $C_N(t)$, d(t), and p(t) versus time data

II. Set: α=.01

E=1E-6

$t_{max} = 100$

N=100

$T = 0.8\ t_{max}$

$a = \alpha - \ln(E)/2T$

III. Set: x = a

$y_k = k\pi/T$, k = 0, 1.....N

IV. For each value of (x,y_k) , k = 0, 1....N perform the following:

1. Compute $B_{1R}(x,y_k)$, $B_{2R}(x,y_k)$,.....$B_{6R}(x,y_k)$ and $B_{1I}(x,y_k)$, $B_{2I}(x,y_k)$,.....$B_{6I}(x,y_k)$ using Equations (19)

2. Compute $C_{NR}(x,y_k)$, $C_{NI}(x,y_k)$, $D_R(x,y_k)$, $D_I(x,y_k)$, $P_R(x,y_k)$, and $P_I(x,y_k)$ using Equations (28a)

3. Compute $Q_{1R}(x,y_k)$, $Q_{1I}(x,y_k)$, $Q_{2R}(x,y_k)$, and $Q_{2I}(x,y_k)$ using Equations (30)

4. Compute $\gamma_R(x,y_k)$ and $\gamma_I(x,y_k)$ using Equations (23)

V. For Each Time, t, of Interest Compute $\Gamma(t)$ using Equation (22)

Figure 12. Flow Chart for Computing Inverse Laplace Transform using Strain Gauge and Displacement Data.

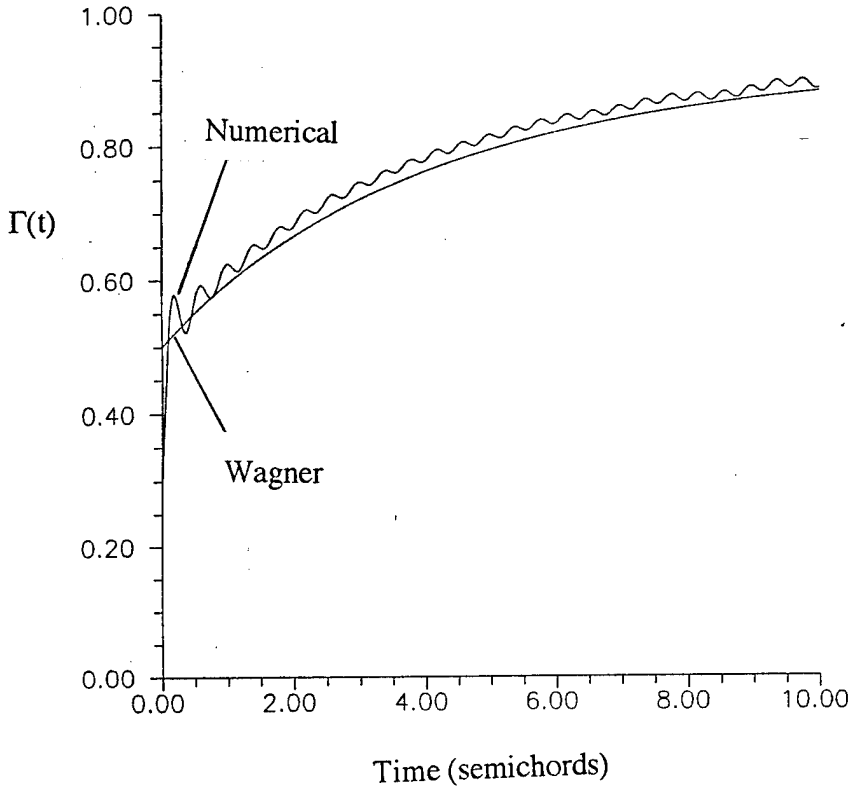

Figure 13. Indicial Response Results for Strain Gauge and Displacement Data Input using Ref.[11], α=0.01, N=200, E=1e-6, t_{max}=100.

displacement data from the accelerometer data as has been described in relation to the results of Figure 11b. Nevertheless, the agreement is still very good.

Part III: Experimental Studies

This section incorporates the use of experimental strain gauge data in the inverse aeroelastic model described above. The strain gauge data were taken as described in the introduction to this report and in detail in Reference[4].

Simplified Aeroelastic Model

The aeroelastic model described in Parts I and II of this report has been simplified by considering the NDOF1 mode only. This simplifies the formulation in that the generalized coordinates for the NDOF2 and TDOF are no longer required. This yields the Laplace transformed aeroelastic reciprocal equations for the indicial response $\gamma(s)$ and the NDOF1 generalized coordinate $Q_1(s)$:

$$\gamma(s) = \frac{B_1(s)Q_1(s) + B_2(s)P(s)}{B_3(s)Q_1(s) + B_4(s)P(s)} \tag{32}$$

and

$$Q_1(s) = \frac{[A_1(s) + A_2(s)\,\gamma(s)]\,P(s)}{A_3(s) + A_4(s)\gamma(s)} \tag{33}$$

where $A_1(s)$-$A_4(s)$ and $B_1(s)$-$B_4(s)$ are functions of the Laplace variable only and may be deduced from Equations 16 and 17 or alternatively from the Equations 3 through 10 by neglecting the NDOF2 and the TDOF coordinates. By separating the above Equations into real and imaginary parts as has been described, either Equation may be inverted to the time domain to obtain either $\Gamma(t)$ or $q_1(t)$ using the numerical procedure outlined in the previous section. For introducing the experimental strain gauge data in Equation 32, $q_1(t)$ is obtained using Equation 29c (neglecting q_2), and $p(t)$ is the experimental angle of attack. The simplified model eliminates the need for a second measurement for obtaining $q_2(t)$ as in the previous section. In Equations 32 and 33, the Laplace transforms $Q_1(s)$, $\gamma(s)$, and $P(s)$ are computed numerically using Equations 28.

Figure 14 illustrates the effect of neglecting higher modes on the sensible force at the strain gauge. The solid curve illustrates the sensible force considering higher modes as heretofore described and the broken line illustrates the simplified model. As expected, the simplified model does not exhibit higher frequency coupling. The two curves would be expected to have similar (numerical) Laplace transforms.

Validation of Reciprocal Model

In this section experimental strain gauge data are used to compute $Q_1(s)$ and angle of attack data are used to compute $P(s)$ to obtain the indicial response $\Gamma(t)$ via Equation 32 and the numerical inversion method of Reference[11]. This indicial response solution is used to compute $\gamma(s)$, which is then used in

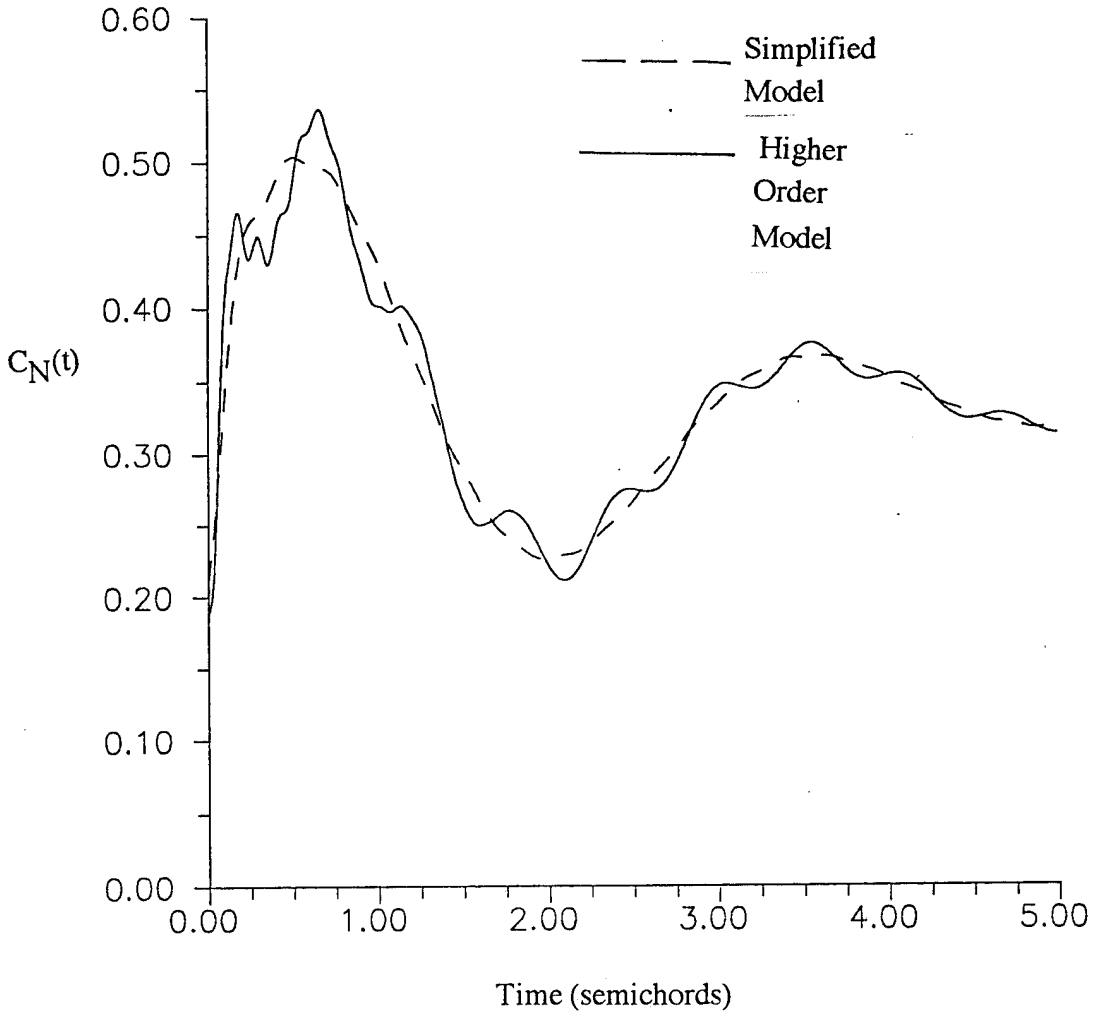

Figure 14. Comparison of Sensible Force using Simplified Model with Higher Order Model.

Equation 33 to reproduce the reciprocal solution for $q_1(t)$. This reciprocity provides a validation of the model and a measure of aeroelastic effects.

Figure 15a illustrates angle of attack data for a step onset of 2°. The initial onset angle has been subtracted off so that the initial angle is shown as zero. The Figure illustrates two separate runs with one step up (increasing α) and one step down. Here attention is focused on the step up case. Figure 15b illustrates $q_1(t)$ data computed from the strain gauge data using Equation 29c. The initial values have again beep subtracted off. Figure 16a illustrates the numerical solution for the indicial response as well as the indicial response computed directly from the strain gauge data using: $T(t) = C_N(t)/\Delta\alpha$. Here the numerical indicial response is multiplied by the steady state slope $C_{N\alpha}$ (= 8.0/rad) which was measured independently in steady alpha tests. It can be seen that after about one semichord the numerical solution tracks the mean of the experimental results. The experimental result contains some higher frequency oscillations which are not completely understood. The frequency of the oscillations is not close enough to the computed NDOF2 frequency to lead one to the conclusion that these are associated with the NDOF2 bending mode. The oscillations may be associated with roughness and/or misalignment in the tow tank track. Nevertheless, the results indicate the the effects of aeroelasticity on the strain gauge output are predominately confined to a small period shortly after the step input. Figure 16b illustrates the reciprocal numerical result for $q_1(t)$ obtained using the numerical indicial response solution of 16a. The reciprocal solution is in agreement with the experimental input. The numerical result does not contain some of the higher frequency content present in the experimental data which is most likely due to the limited number of terms used in the Fourier inversion routine. It is worth noting in Figure 16a that the numerical inversion routine predicts half the initial value at time zero, which is a consequence of the formulation [11].

Figures 17a and 17b illustrate the reciprocal pair using the experimental data of Figures 15a and 15b for the step down case. As seen in Figure 17a, the effects of aeroelasticity are confined to times below five semichords.

Central Difference Formulation for the Indicial Response

Ideally the indicial response for the step up and step down cases would be identical. Comparisons of Figures 16a and 17a indicates some differences between the two cases. These may be due in part to slightly different onset conditions and aerodynamic reactions to the step. In each case the step height was approximately one degree and the nondimensional pitch rate was about 0.15. The effective angle of attack at the leading edge in the step up and step down cases during the pitch motion are significantly different due to the wash induced by the pitch motion. Subsequent boundary layer and wake formation may be influenced by these events.

To account for differences in step up and down results, the indicial response has been computed using a central difference given by:

$$\Gamma(t) = \frac{\Gamma_u(t)\Delta\alpha_d + \Gamma_d(t)\Delta\alpha_u}{\Delta\alpha_u + \Delta\alpha_d} \qquad (34)$$

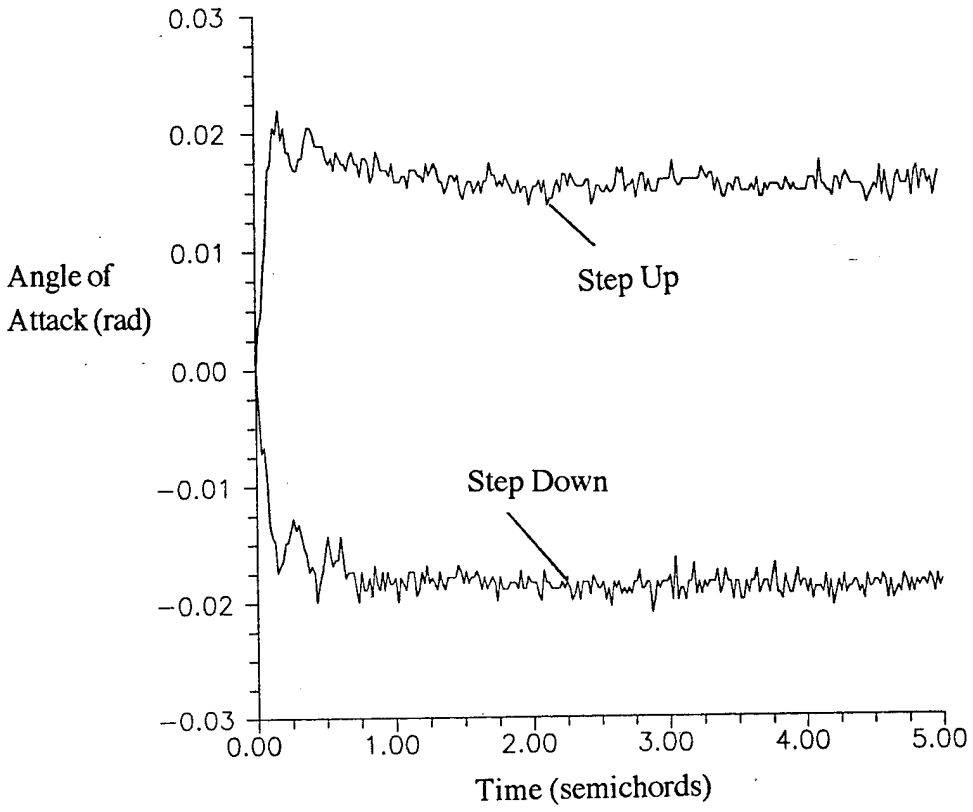

Figure 15a. Angle of Attack Data for Step Up and Step Down Runs for an Onset Angle of 2°.

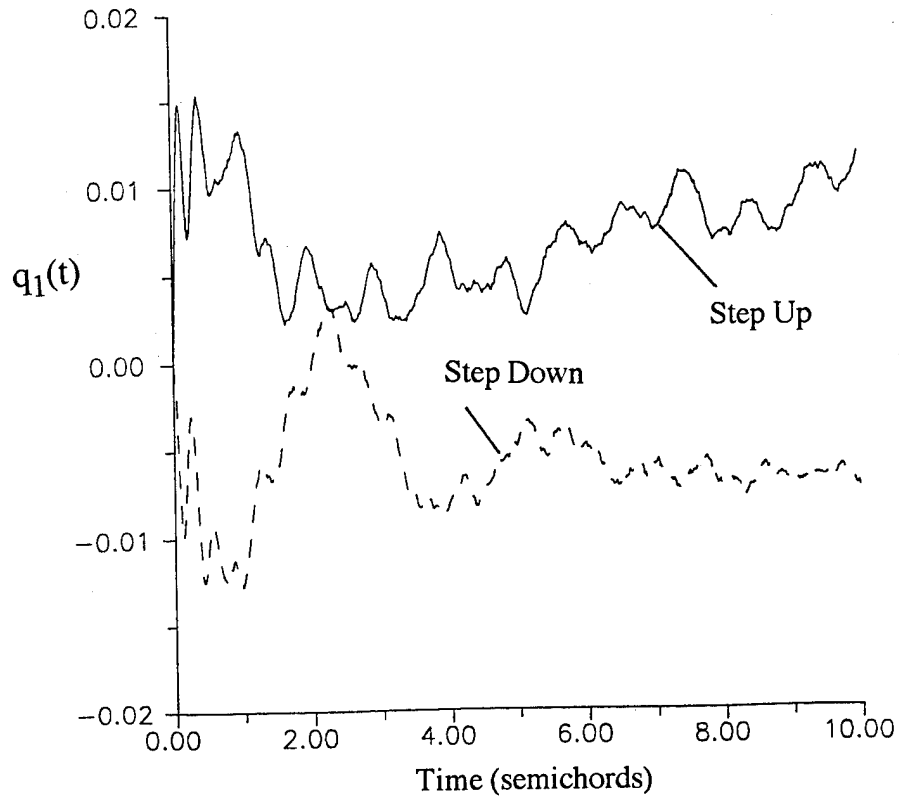

Figure 15b. NDOF1 Results from Strain Gauge Data for Step Up and Step Down Runs for an Onset Angle of 2°.

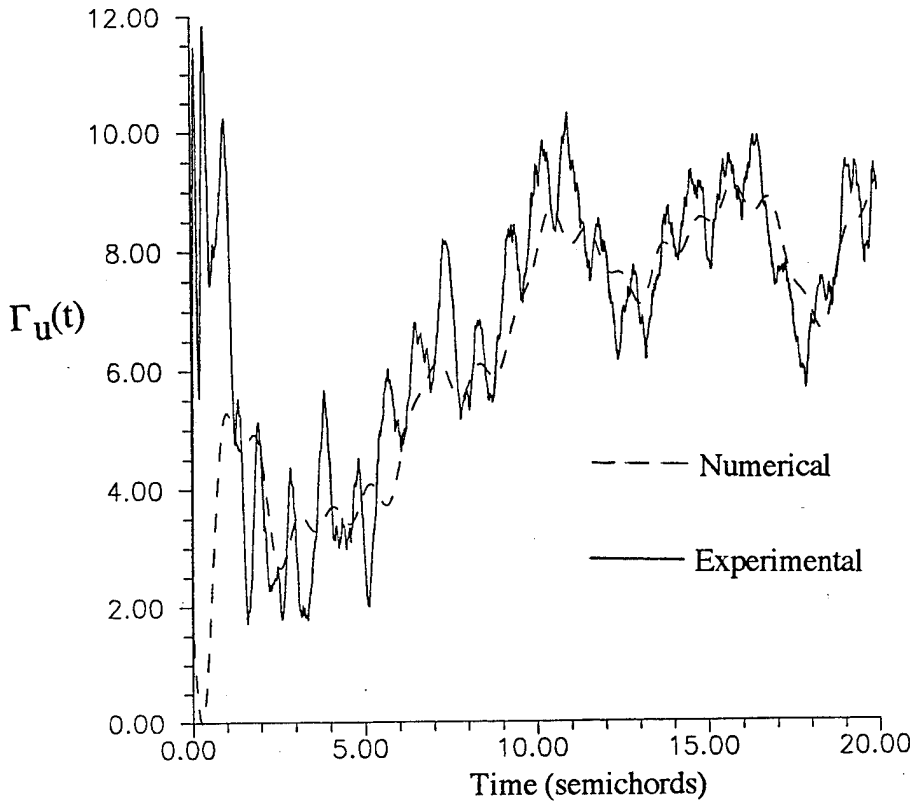

Figure 16a. Numerical Indicial Response Results and Directly Computed Indicial Response for Step Up at an Onset Angle of 2°.

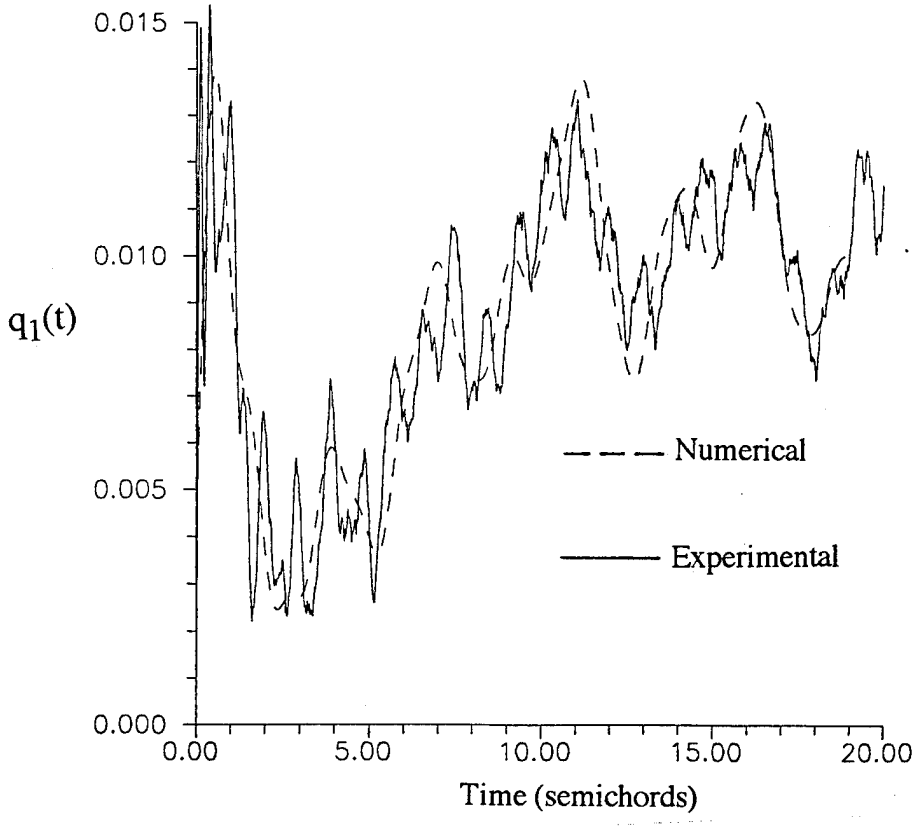

Figure 16b. Reciprocal NDOF1 Generalized Coordinate Results and Directly Measured NDOF1 Data for Step Up at an Onset Angle of 2°.

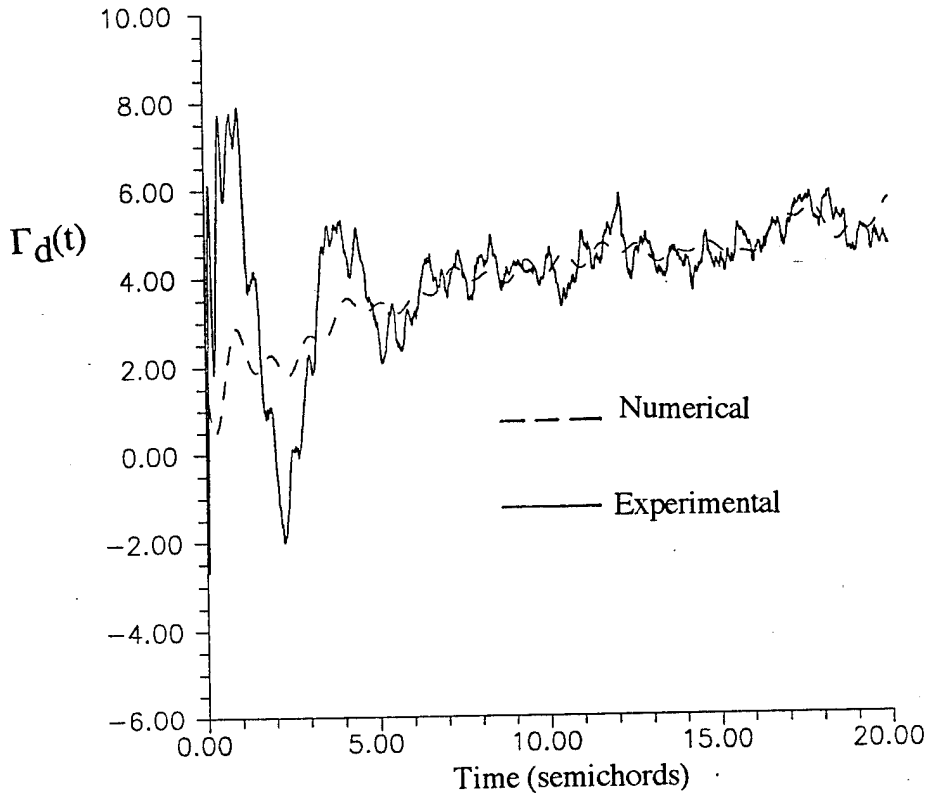

Figure 17a. Numerical Indicial Response Results and Directly Computed Indicial Response for Step Down at an Onset Angle of 2°.

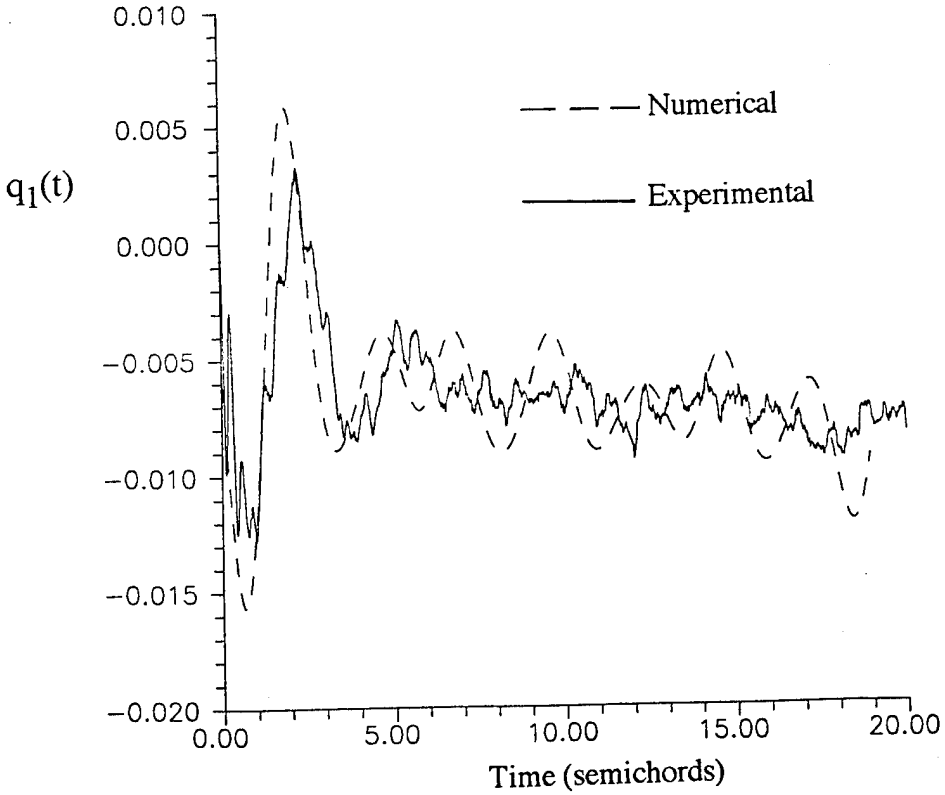

Figure 17b. Reciprocal NDOF1 Generalized Coordinate Results and Directly Measured NDOF1 Data for Step Down at an Onset Angle of 2°.

where the subscript "u" refers to step up and "d" to step down. The central difference results are shown in Figure 18 along with the theoretical result of Wagner. The present result indicates a smaller indicial response than that predicted by Wagner.

Figure 18 indicates that the effects of aeroelasticity are strongest below about two semichords after the step. This is due to the large inertial loads generated by the rapid step input. This is an important result when considering that it is not necessary to experimentally impart rapid step-like input motions as has been done in the present tow tank studies in an attempt to directly measure the indicial response. It should only be necessary to consider small amplitude motions which are locally linear in the indicial response (i.e. the response is the same over the motion amplitude). Such a motion might include a more gradual small amplitude ramp. This type of motion would not involve the large inertial loading experienced in the present rapid step motions and may give better results. The use of a rapid step motion was motivated in earlier tests designed to directly measure the indicial response which is defined for a step input. The present aeroelastic formulation does not require a rapid step input. The present method for determining indicial responses would appear to be applicable to wind tunnel rigs and three dimensional rigs so long as the aeroelastic equations are valid.

High Angle of Attack Case

This section describes the treatment of experimental step up and step down cases for an onset angle near 17°. The principal difficulty in the higher angle case is the validity of the aerodynamic loading terms in the equations of aeroelasticity, and in particular the so-called noncirculatory terms. The discussion below deals with a simple method for estimating the noncirculatory loads using one of the modal aeroelastic equations. Below attention is focused on the NDOF2 Equation 3b which is of the form:

$$M_2\ddot{q}_2 + K_2q_2 = c_1\dot{p} + c_2\ddot{p} - c_3\ddot{q}_1 - c_4\ddot{q}_2 + \text{circulatory terms} \tag{35}$$

where c_1 through c_4 are constants and the circulatory terms are formulated in terms of the convolution integral. In the linear case the constants c_1 through c_4 all contain the two dimensional noncirculatory aerodynamic loading term, π, multiplied by structural terms (mode shapes) which arise in formulating the uncoupled generalized Equation (see Equations 5-7). If one of the constants is known, each of the other constants may be computed therefrom from the known structural properties.

The constant c_4 may be combined with M_2 and thus the term apparent mass. The free vibration response is therefore governed by:

$$(M_2 + c_4)\ddot{q}_2 + K_2q_2 = 0 \tag{36}$$

which has a harmonic solution with a frequency of vibration given by:

$$\omega_2 = \sqrt{\frac{K_2}{M_2 + c_4}} \tag{37}$$

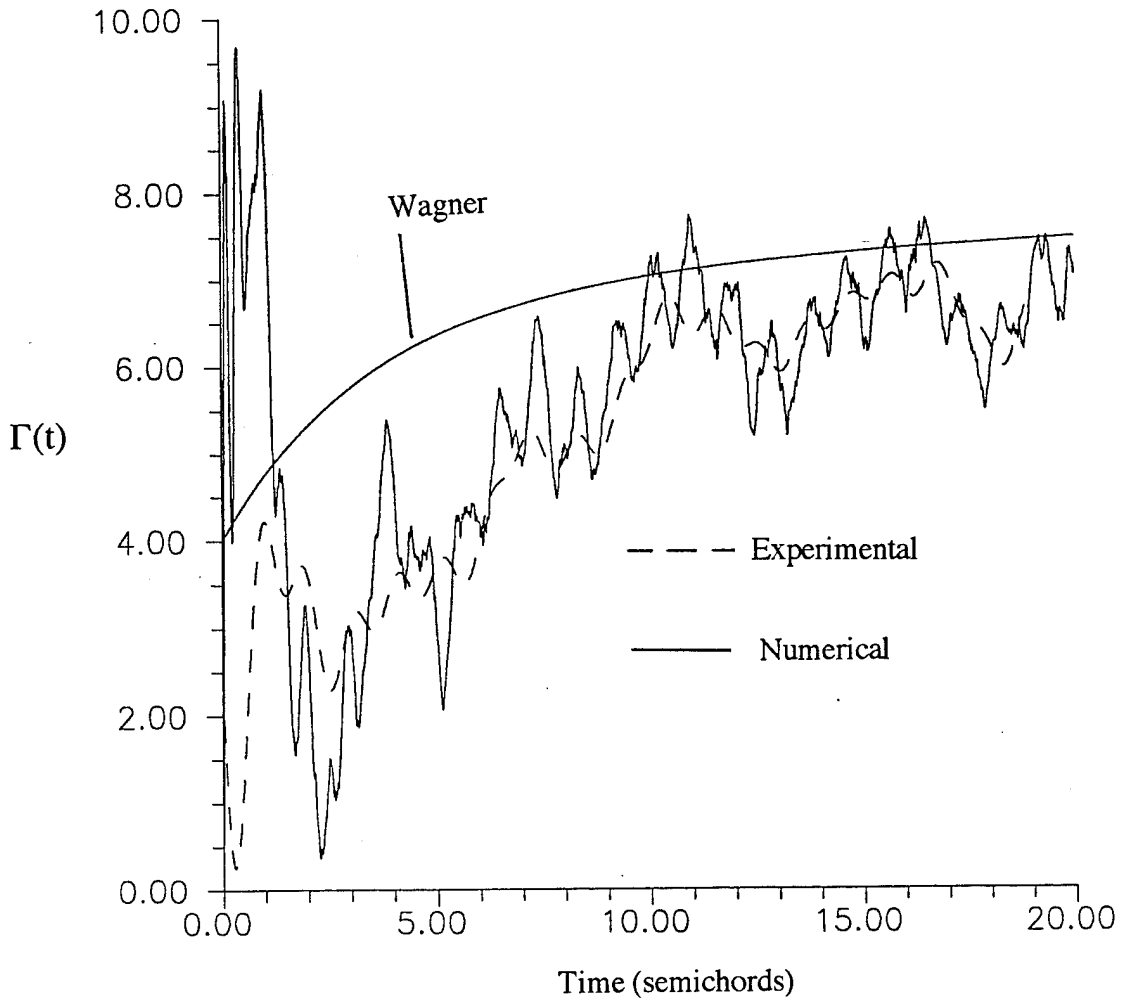

Figure 18. Numerical Indicial Response Results for a Step Onset Angle of 2° Using a Central Difference Formulation.

Thus, assuming the structure is linear so that K_2 and M_2 are constants, a measurement of ω_2 would allow one to compute the the apparent mass c_4 using Equation (37). The remaining constants c_1 through c_3 may be computed from c_4. The algebra is left to the interested reader.

An accelerometer located on mass element 13 has been used to measure the frequency response of the test rig at various step onset angles of attack. A FFT was performed on the accelerometer signal and the power spectral density has been computed. The power spectral density is simply the magnitude of the complex Fourier coefficients [7]. The results for onset angles of 2° , 11°, and 25° are illustrated in Figure 19. Recalling that the NDOF2 aeroelastic frequency based on linear airfoil theory was around 12 rad/semichord, it is seen that the NDOF2 response occurs at nearly the same frequency in all three cases. This suggests that the apparent mass and/or noncirculatory loading at higher angles of attack may be similar to that for the linear low angle case. These results are preliminary and presented here as conjecture.

Using the same governing equations as in the linear case, and analyzing experimental data for an onset angle of 17° in a way parallel with that described above for the 2° onset case yields the indicial response shown in Figure 20. These results are based on the central difference formulation above involving both a step up and a step down run. Again it appears that aeroelastic reactions ar strongest for times below about two semichords.

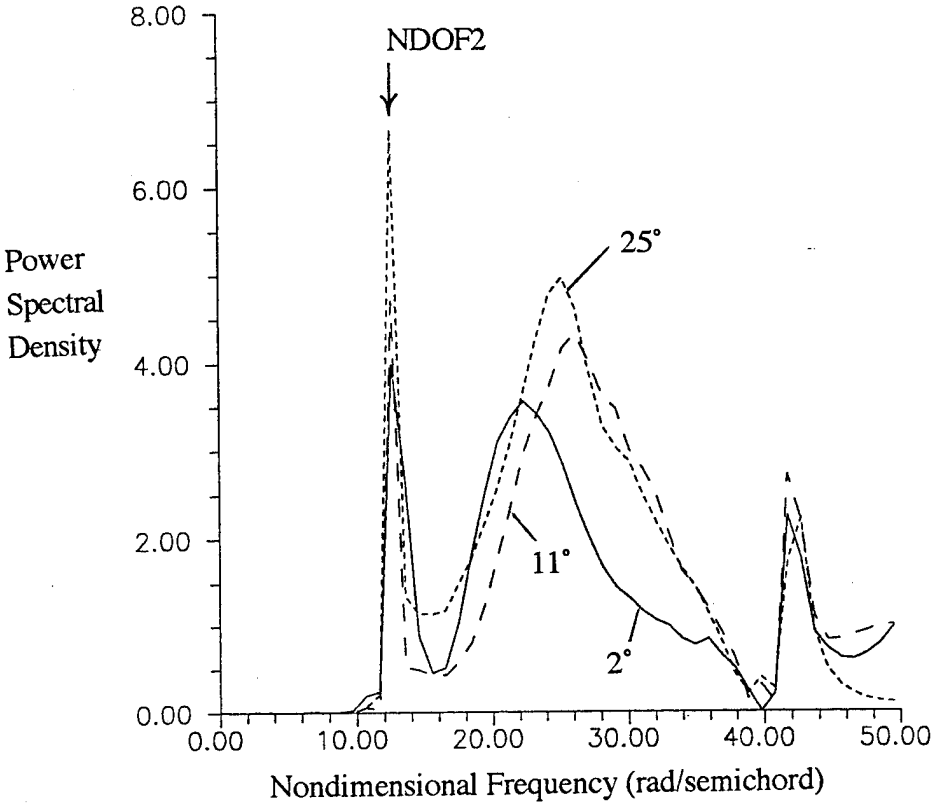

Figure 19. Power Spectral Density Distribution for High and Low Onset Angles.

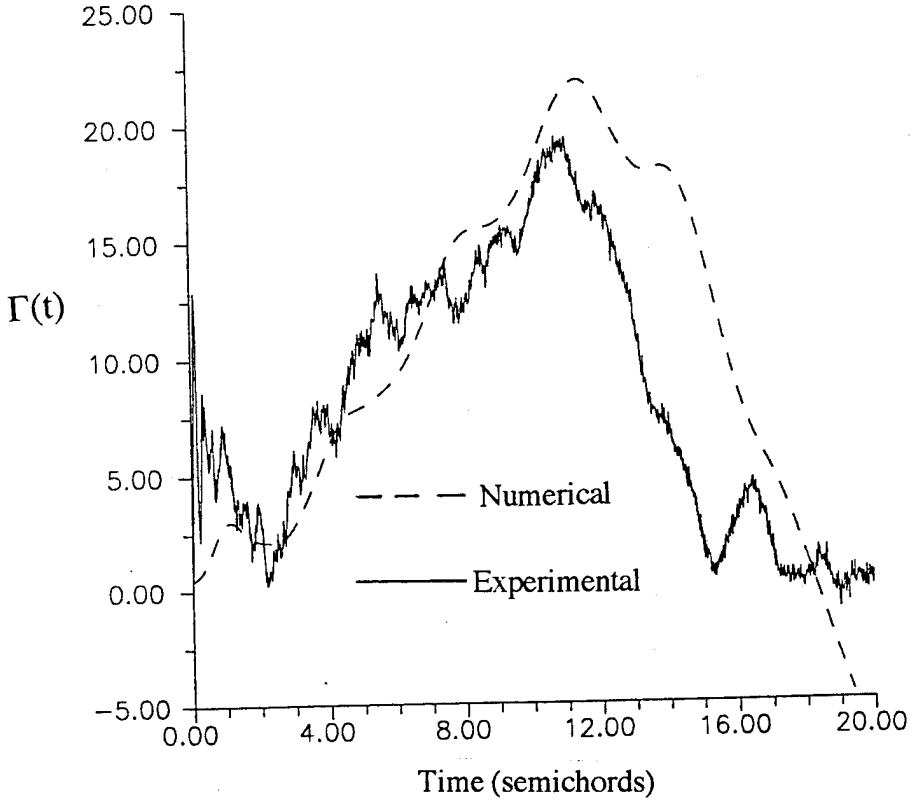

Figure 20. Numerical Indicial Response Results for a Step Onset Angle of 17° Using a Central Difference Formulation.

Conclusion

The research described herein has focused on two areas. The first is a detailed aeroelastic analysis of an airfoil test rig undergoing rapid motion at low incidence. The analysis has led to a relatively general method to solve the differential equations of aeroelasticity in closed form using Laplace transforms and state-of-the-art computer software(MACSYMA) for performing the required algebraic operations. The results indicate that aeroelastic reactions may have a significant effect of strain gauge data and should be considered in experimental design of the type described as well as subsequent data reduction.

The second area of research has been directed towards developing a method to determine the airfoil indicial response from typical aerodynamic measurements such as strain gauge and accelerometer data. The method is essentially a solution of the equations of aeroelasticity expressed in reciprocal form for the indicial response given the aeroelastic response. Because the method is directed to the reduction of experimental data in discrete form, a numerical method has been used. The method provides a theoretically sound approach for determining an indicial response experimentally, even though the indicial response is defined for an instantaneous step of diminishing amplitude. It has been shown that given an aeroelastic response computed using Wagner's function, the inverse method correctly determines the indicial response to be Wagner's function. The method has been applied to a limited number of experimental cases as well. The method may have applications for other types of systems such as heat transfer and pure structural modeling as the governing equations are similar in form.

The author believes that the type of research described in this report can provide guidance in the design of future experiments. It is anticipated that an experimental apparatus could be designed to circumvent some of the difficulties encountered using the present rig. For example, it should be possible to design a structure for which it is necessary to consider only a single mode of vibration, as opposed to the system of three modes given by Equations (3a)-(3c). Also, the fact the present airfoil was pitched about the quarter chord simplifies the formulation for the aerodynamic moments. Furthermore, it was necessary to consider the normal/torsional coupling in the aeroelastic analysis primarily because the center of mass of the airfoil was not on the pitch axis. It should be possible to judiciously add mass to the test rig so that the center of gravity would coincide with the pitch axis to minimize these effects. Finally, as has been noted, it is not necessary to experimentally impart rapid step-like input motions as has been done in the present tow tank studies. The rapid step-like motions were motivated by attempts to directly measure the indicial response which is defined theoretically for a step motion. It is only necessary to consider small amplitude motions which are locally linear in the indicial response. Such a motion might include a very gradual small amplitude ramp. This type of motion will not involve the large inertial loading experienced in the present rapid step motions. The present method for determining indicial responses would appear to be applicable to , tow tunnel rigs, wind tunnel rigs, and three dimensional rigs as well so long as the aeroelastic equations can be accurately formulated.

Future work may focus on using the present approach to determining the indicial response over a range of onset angles of attack, and using the responses in a numerical convolution integral to predict large amplitude motions such as ramp motions for which baseline experimental data exist for comparison. This should further provide validation of the indicial responses.

Acknowledgement

This work was supported under AFOSR Grant F49620-93-0030. The author is grateful to Mr. Jerry E. Jenkins of Wright Laboratories for his many valuable suggestions during this project.

References

[1]Bisplinghoff, R.L., Ashley, H., and Halfman, R.L., *Aeroelasticity*, Addison-Wesley, Boston, Mass., 1957.

[2]Chow, C.Y. and Huang,M.K., "The Initial Lift on an Impulsively Started Airfoil of Finite Thickness," J. Fluid Mechanics, vol. 118, pp. 393-409, 1982.

[3]Beddoes, T.S., "Practical Computation of Unsteady Lift," Vertica, vol. 8, pp. 55-71, 1984.

[4]Graham, G. M., Islam, M. and Jenkins, J. E.,"Nonlinear Normal Force Indicial Responses for a 2-D Airfoil," AIAA Paper No. AIAA-91-2866-CP, New Orleans, La., Aug. 12-14, 1991 .

[5]Tobak, M. and Schiff, L.B., "Aerodynamic Mathematical Modeling-Basic Concepts," AGARD Lecture Series No.114, Paper 1, March 1981.

[6]Kaplan, W.K., *Advanced Calculus*, Addison-Wesley Publishing Co., 2nd ed., pp. 515-521.

[7]Clough, R.W. and Penzien, J., *Dynamics of Structures*, McGraw Hill Publisher, 1975.

[8]Fung, Y.C, *An Introduction to the Theory of Aeroelasticity*, Dover Publications, New York, 1969.

[9]Higdon, A. et al., *Mechanics of Materials*, Wiley and Sons, Inc. Publisher, New York, 1960.

[10]Burden, R.L., Farres, J.D., and Reynolds, A.C., *Numerical Analysis*, Prindle, Weber & Schmidt Boston, Ma., 1980, p.185.

[11]Crump, K.S., "Numerical Inversion of Laplace Transforms Using a Fourier Series Approximation," Journal of the Association for Computing Machinery, Vol. 23, No. 1, Jan. 1976, pp.89-96.

[12]Weeks,W. T., "Numerical Inversion of Laplace Transforms Using Laguerre Functions," Journal of the Association for Computing Machinery, Vol. 13, No. 3, July 1966, pp.419-426.

Appendix A

This Appendix gives the values of the constants appearing in Equations (19a)-(19f).

$b_1 = 20.5091$	$b_9 = -3.4639$	$b_{17} = 6.7969$
$b_2 = 113.576$	$b_{10} = -25.4171$	$b_{18} = 15.2134$
$b_3 = -16.7068$	$b_{11} = -14.7368$	$b_{19} = 64.7242$
$b_4 = -9.6866$	$b_{12} = 49.8633$	$b_{20} = -126.9761$
$b_5 = 3.6241$	$b_{13} = 54.0083$	$b_{21} = -190.8867$

$b_6 = 1143.83$ $b_{14} = 14.5516$ $b_{22} = -63.9107$

$b_7 = -2.6691$ $b_{15} = -44.9456$

$b_8 = -5.9743$ $b_{16} = 42.5436$